

# CHALMERS



## Component Synthesis of Machine Tool and Cutter for Process Optimisation

ANDERS LILJEREHN

Department of Applied Mechanics  
CHALMERS UNIVERSITY OF TECHNOLOGY  
Gothenburg, Sweden 2012



THESIS FOR THE DEGREE OF LICENTIATE OF ENGINEERING  
IN SOLID AND STRUCTURAL MECHANICS

Component Synthesis of Machine Tool and  
Cutter for Process Optimisation

ANDERS LILJEREHN

Department of Applied Mechanics  
CHALMERS UNIVERSITY OF TECHNOLOGY

Gothenburg, Sweden 2012

Component Synthesis of Machine Tool and Cutter for Process  
Optimisation

ANDERS LILJEREHN

©ANDERS LILJEREHN, 2012

Thesis for the degree of Licentiate of Engineering 2012:08

ISSN 1652-8565

Department of Applied Mechanics

Chalmers University of Technology

SE-412 96 Gothenburg

Sweden

Telephone: +46 (0)31-772 1000

Chalmers Reproservice  
Gothenburg, Sweden 2012

Component Synthesis of Machine Tool and Cutter for Process Optimisation  
Anders Liljerehn  
Division of Dynamics  
Department of Applied Mechanics  
Chalmers University of Technology

## Abstract

Metal cutting is today one of the leading forming processes in the manufacturing industry. The metal cutting industry houses several actors providing machine tools and cutting tools with a fierce competition as a consequence. Extensive efforts are made to improve the performance of both machine tools and cutting tools. Performance improvements are not solely restricted to produce stronger and more durable machine tools and cutting tools. It also includes knowledge about how the machine tools and cutting tools should be used to perform at an optimum of their assembled capacity. This work presents a methodology to synthesise the dynamic behaviour of a machine tool and cutting tool assembly based on component models of the machine tool and the cutting tool. To treat the structure as an assembly of subcomponents aims first of all to reduce measurement effort to get the receptance at the tip of the machine tool/cutting tool which is needed for process stability optimisation. This methodology compares to today's state of the art methodology which require experimental modal analysis (EMA) for each cutting tool of interests mounted in the machine tool. The subcomponent approach presented here limits the EMA to the machine tool component. The machine tool component model is then connected to a component FE-model of the cutting tool of interest. The subcomponents models are obtained and coupled based on state-space formulation, a technique that is new to component synthesis of machine tool/cutting tool structures. A sensitivity analysis is also presented to raise awareness of crucial parameters that influences the result of the synthesised system. The understanding about how to assign cutting process parameters in order to optimise a cutting operation with respect to machining stability is of utmost importance to provide good productivity and process stability. This methodology opens windows not only to optimisation of an existing cutting tool but it also permits tailored cutting tool solutions for existing machining operations.

Keywords: Metal Cutting, Component synthesis, Chatter stability, Receptance coupling, System Identification, State-space models, Experimental modal analysis



*To my loving family:  
Helena, Stina and Ludvig*



## PREFACE

This thesis is the result of the work conducted during 2009-2012 within the project *Using predictions to avoid chatter in cutting operations* at the Department of Applied Mechanics, Division of Dynamics at Chalmers University of Technology. The project is financed by Sandvik Coromant and the Centre for Advanced Production Engineering (CAPE). The completion of this thesis owes to the following persons: My supervisor Professor Thomas Abrahamsson with his expertises within my research field and his ability to guide me in the right direction. He who always saw the positive side of my problems and always cheered me up when everything seemed hopeless. Mikael Lundblad, Head of the department Coromant Tooling Metal cutting Research (CTMR) without whom I probably never would have the opportunity to conduct this research. To my wife Helena without whom this project would have never been completed. For here patience, support and love. To my children Stina and Ludvig for greeting me with their smiles when I come home from my work and my travels and always keeping me grounded. To Per Sjövall who helped me with and allowed me to use his state-space coupling routines. To Anders T Johansson and Martin Magnevall for their help and support during this work and finally to Jon Nödtveidt for accompanying me during my travels to Gothenburg.



# THESIS CONTENT

This thesis consists of an introduction and is based on the following appended papers:

**Paper A** A. Liljerehn, A. T. Johansson, T. Abrahamsson, Dynamic substructuring in metal cutting machine chatter. Presented at *ISMA 2010 Conference on Noise and Vibration*

**Paper B** A. Liljerehn, T. Abrahamsson, Experimental–Analytical Substructure Model Sensitivity Analysis for Cutting Machine Chatter Prediction. Presented at the *30th International Modal Analysis Conference 2012*

The appended papers were prepared in collaboration with co-authors. The author of this thesis was responsible for the major progress of work, including taking part in planning the papers, developing the theory, developing and carrying out measurements, the numerical implementations and writing the reports.



# Contents

<b>Abstract</b>	<b>i</b>
<b>Preface</b>	<b>v</b>
<b>Thesis content</b>	<b>vii</b>
<b>Contents</b>	<b>ix</b>
<b>I Extended summary</b>	<b>1</b>
<b>1 Introduction and motivation</b>	<b>1</b>
1.1 Aim and scope . . . . .	2
<b>2 Chatter vibrations in metal cutting</b>	<b>3</b>
2.1 Chatter in turning of a disk . . . . .	3
2.1.1 Stability lobe diagrams in turning . . . . .	4
2.2 Chatter in milling . . . . .	8
2.2.1 Stability lobe diagrams in milling . . . . .	8
2.3 Time domain chatter stability boundary . . . . .	12
<b>3 Machining dynamics by component synthesis</b>	<b>13</b>
<b>4 Component synthesis theory</b>	<b>16</b>
4.1 Component mode synthesis . . . . .	16
4.2 FRF based coupling . . . . .	17
4.2.1 Impedance coupling method . . . . .	17
4.2.2 Generalised FRF impedance coupling technique . . . . .	19
4.3 State-space based coupling . . . . .	20
<b>5 Summary of appended papers</b>	<b>20</b>
<b>6 Conclusions and future work</b>	<b>21</b>
<b>References</b>	<b>21</b>
<b>II Appended papers A-B</b>	
<b>Paper A</b>	<b>A1-A15</b>
<b>Paper B</b>	<b>B1-B14</b>



## Part I

### Extended summary

#### 1 Introduction and motivation

The strong competition in manufacturing industry has led to a constant search for efficient cutting operations to reduce cost. Increased productivity require faster machining and lower cycle times. In order to meet these demands it is desired that process parameters, such as cutting speed, feed velocity and depth of cut are taken to the next level. As a consequence of modified process parameters, an increase in cutting forces and temperature in the cutting zone follows. Elevated process temperatures and cutting forces accelerates tool wear and may contribute to work piece distortion. Increased cutting forces also make the machining process more prone to regenerative vibrations. This phenomenon is known as chatter.

Chatter vibrations compromises the quality of the machined work piece surface, it may break the cutting tool, and in extreme cases it may lead to damage of the machine tool. To predict and optimise the cutting process, in which the avoidance of chatter is central, an accurate representation of the dynamic properties of the machine and cutting tool assembly is of the essence. Extensive research has been ongoing on the topic of chatter and regenerative vibrations in metal machining with pioneering work conducted in the 1960's by Thustly [1] and Tobias [2]. Both [1] and [2] presented similar solutions to analytical expressions predicting the stability limit with respect to depth of cut of a turning operation. Their theoretical framework for turning operations were later developed further by Budak and Altintas [3, 4] to be applicable for milling as well. In their work, a dynamic milling model with directional dynamic milling force coefficients were introduced enabling an analytical solution that better considered the change in direction of the cutting force in a milling operation. The analytical solution to the stability problem in metal machining presented in reference [1–4] all set out from the assumption that the cutting forces has a linear dependency with respect to feed,  $f$ , and depth of cut,  $a_p$ . Unfortunately, this approximation is not always proper. Phenomena like cutting tool jumping in and out of cut during vibrations and relations between cutting force and chip thickness that are non-linear are examples that may change the prediction of the stability limit in a way that cannot be explained by the analytical solution. A time domain stability chart, see references [5–14], is one way of permitting a non-linear solution of the machining stability, However, such are often far more time consuming to establish.

Regardless of methodology chosen to predict the stability boundary for a cutting process it is essential to know the frequency response function (FRF) at the tool tip of the machine tool mounted cutting tool. The state-of-the-art is to obtain the required FRFs at the tool tip by EMA. In the case of a process optimisation of a multi-operational machine tool, this approach requires physical testing of a multitude of machine-tool/cutting tool combinations. The downside to this approach is that not only is it required to obtain the FRFs for all cutting tools of interest, since the dynamic properties changes with the variation in geometric properties for the different cutting tool, but it also requires that the machine tool is still standing during measurements. This results in loss of valuable production time.

A way of reducing measurement time is to utilise receptance coupling technique to synthesise the dynamic response at the tool tip. The advantage of the receptance coupling technique is that a mechanical system, in this case the machine tool with the mounted cutter, can be viewed as an assembly of subsystems. This approach allows the frequency response to be obtained from substructuring based on a mixture of measurements, modelling and analysis depending on what suits best to the substructure in question. Modelling of a machine tool structure is hard because of its mechanical complexity, and the substructure is therefore preferably obtained through system identification to create a system description based on measurements. The less complex cutting tool can be modelled by finite elements, sometimes with as simple elements as Timoshenko beam elements [4].

### 1.1 Aim and scope

In this project, the use of a rational combination of experimental and analytical modelling is made to characterise the dynamic properties of the system. This approach may lead to a more time and cost efficient optimisation. The project aims at characterise the dynamic properties of the interface between the machine tool spindle and a cutting tool in a machine tool/cutting tool assembly. The information about the spindle interface, in combination with FE-analysis of the cutting tool will give the information needed for determining optimised design with a best set of cutting data to avoid regenerative vibrations. Such optimisation aims at maximising productivity, process stability, reliability and reduce dynamic testing.

Characterisation of the spindle interface in the machine tool will here be done through inverse modelling of the dynamic behaviour. The characterisation of the dynamic properties at the interfaces between the tool and work piece will

be made using system identification procedures. This information, together with *e.g.* finite element modelling of the tool, can be used to determine the cutting properties that give a chatter-free operation. In the sequel, this may be used for discussion of optimisation of productivity and cutting tool design.

The machine tool is a complex mechanical structure which is assembled with numerous mechanical joints. This makes it difficult to model with FEM since the dynamic properties at the joints are hard to foresee. The joints may also carry non-linearities that makes the modelling very cumbersome. For testing, the structure is also hard to excite with sufficient force to cover the desired frequency range for a proper EMA. Though the overall objective is to overcome these obstacles, the scope of the work presented in this thesis has been restricted to application of the coupling routines to a test rig, see **Paper A**. Method verification and parameter sensitivity analysis have been restricted to analytical machine tool representations, see **Paper B**.

## 2 Chatter vibrations in metal cutting

Chatter vibrations can occur in all metal cutting processes and is one of the most common productivity limiting factors in metal machining. Chatter occurs from dynamic force feed-back due to variation in chip thickness during cut. The variation in chip thickness originates from a phase shift in vibration marks left on the machined surface between two consecutive cuts. This phase shift is dependent on the dynamics of the machine tool/cutting tool assembly. The spindle speed  $n$  and number of cutting teeth  $z$  govern the period time between cuts. Since the spindle speed is a process parameter to be selected by the operator, this parameter can be chosen so that the vibration marks from the previous cut is in phase with the current cut. If the vibration marks between cuts is in phase then there will be no force feed-back and there will be no regenerative vibrations. A process of optimisation with support of modelling and analysis is possible provided that the vibrational frequency of the tool tip is known.

### 2.1 Chatter in turning of a disk

The simplest explanation model of chatter vibrations in the cutting process do regard orthogonal turning of a disk where the tool is fed in the radial direction of the disk. In case of a completely stable cutting process this example would provide that the feed,  $f_n$ , and the uncut chip thickness  $h_D$ , would be the same. However, if we consider the tool to be flexible in the feed direction and we have a vibration which may be initiated from the entry of the cutting tool, the

lamina formation of the chip or hardness variations in the work piece material can cause forced oscillations. The vibration of the cutting tool will then leave a wavy surface imprinted on the work piece. When the work piece has turned one full revolution this waveform on the surface will result in a variation in chip thickness,  $h_D(t)$ , provided that there is a phase shift,  $\epsilon$ , between the previous and the currently cut surface. The time dependent chip thickness,  $h_D(t)$ , is in this case no longer constant with the feed per revolution  $f_n$ , of the cutting tool. The resultant chip thickness will instead be a function of the feed per revolution  $f_n$ , the inner modulation, *i.e* current cut surface,  $y(t)$  and the outer modulation, *i.e* previously cut surface,  $y(t - \tau)$ , see Figure 1.

The progression of the tool vibration under these conditions can take one of three forms. The first case is a stable form where the vibration is damped out over time and the vibration amplitude diminishes. The second is were the vibration stays critically stable were the vibration amplitude neither dampens out or grows and the third is when the system becomes unstable and the vibrations grows to large levels. The last case is what is known in metal machining as chatter.

### 2.1.1 Stability lobe diagrams in turning

The most interesting case to predict, is the case were the process is critically stable. The first researchers to work actively to predict the stability limit for this turning case were Thustly [1] and Tobias [2] who derived similar linear analytical expressions for prediction of chatter stability. They made a linearisation of the excitation force from the cutting process which permitted the stability equations to be derived in the Laplace domain. From these an analytical expression for stability could be obtained. Both researchers stated that the cutting force acting in the feed direction,  $F_f(t)$ , could be expressed as a proportional relation between the edge length in cut,  $a_p$ , the chip thickness,  $h_D(t)$ , and the work piece material dependent specific cutting force coefficient,  $k_f$ , as

$$F_f(t) = k_f a_p h_D(t) \quad (1)$$

From Figure 1 it can be concluded that the the variation in chip thickness can be expressed as  $h_D(t) = f_n + y(t - \tau) - y(t)$ , with  $\tau$  being the time for one full turn of the work piece. Based on this conclusion the equation of motion of the system can be expressed as

$$m\ddot{y}(t) + c\dot{y}(t) + ky(t) = k_f a_p [f_n + y(t - \tau) - y(t)] \quad (2)$$

The next step to derive an analytical expression for the critical stable system is to take the time invariant Delay Differential Equation (DDE) to Laplace domain. In Laplace domain the current cut is expressed as,  $Y(s) = \mathcal{L}(y(t))$

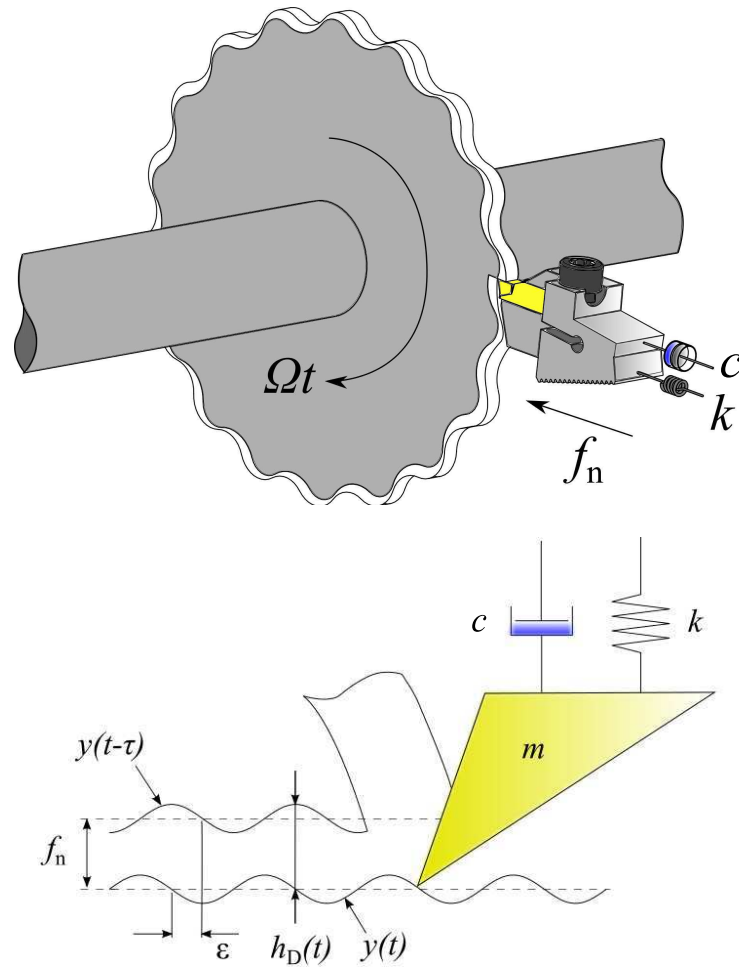


Figure 1: Chip thickness variation in a turning process subjected to regenerative vibrations. The nominal feed is  $f_n$

and the previous cut is expressed as  $Y(s)e^{s\tau} = \mathcal{L}(y(t - \tau))$ . The dynamic chip thickness in Laplace domain is therefore

$$h_D(s) = f_n + Y(s)e^{s\tau} - Y(s) = f_n + Y(s)(e^{s\tau} - 1) \quad (3)$$

and the dynamic cutting force in Laplace domain becomes

$$F_f(s) = k_f a_p h_D(s) \quad (4)$$

The vibration excited by the dynamic cutting force can now be written as

$$Y(s) = F_f(s)H(s) = k_f a_p h_D(s)H(s) \quad (5)$$

where  $H(s) = k + sc + s^2m$  is the transfer function between the dynamic force and the displacement. The relation between the dynamic chip thickness,  $h_D(s)$  and the feed per revolution  $f_n$  can, by substituting the expression of  $Y(s)$  in Equation (5) into Equation (3), be expressed as

$$\frac{h(s)}{f_n} = \frac{1}{1 + k_f a_p H(s)(1 - e^{s\tau})} \quad (6)$$

From Equation (6) the characteristic equation of the closed loop system is found to be

$$1 + k_f a_p H(s)(1 - e^{s\tau}) = 0 \quad (7)$$

The stability limit where the system is critically stable with respect to the edge length in cut,  $a_p^{\text{lim}}$ , can after some manipulation of Equation (7), for details see [15], be shown to be

$$a_p^{\text{lim}} = \frac{-1}{2k_f \Re(H(s))} \quad (8)$$

Here it can be seen that only negative values of the real part of the frequency response function,  $\Re(H(s))$ , produces valid results since  $a_p^{\text{lim}}$  has to be positive. The spindle speed and number of waves left on the work piece surface  $N$ , is related to frequency  $\omega = -js$ , as

$$n = \frac{\omega}{60(2\pi N + \epsilon)} \quad (9)$$

where

$$\epsilon = 3\pi + 2\psi$$

and for negative  $\Re(H(s))$ ,

$$\psi = \begin{cases} -\pi + \tan^{-1} \left| \frac{\Im H}{\Re H} \right| & \text{if } \Im H < 0 \\ -\pi - \tan^{-1} \left| \frac{\Im H}{\Re H} \right| & \text{if } \Im H > 0 \end{cases}$$

Figure 2 shows how the solution of Equation (8) corresponds to the stability limit of the first stability lobe, *i.e.*  $N = 0$ .

A stability lobe diagram for a certain spindle speed interval can now be created by solving Equations (8)-(9) for a sufficient number of lobes  $N$ , see Figure 3. From Figure 3 it can be seen that some spindle speeds are better than others where larger edge lengths in cut,  $a_p$ , can be machined without encountering

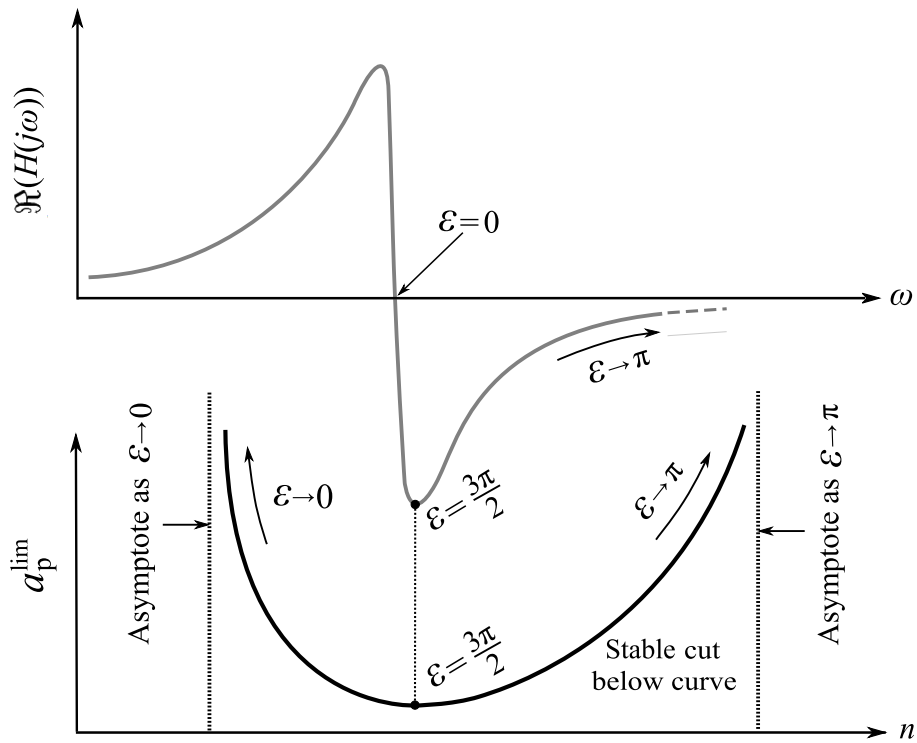


Figure 2: Relation between real part FRF  $\Re(H(j\omega))$  and stability lobe for  $N = 0$

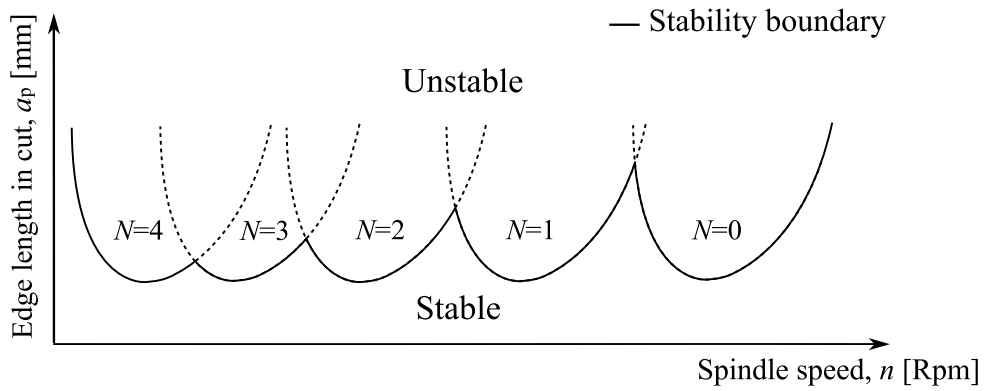


Figure 3: Stability lobe diagram

chatter. It can also be seen that for higher numbers of surface waves the closer the lobes get and the lesser the stability boundary for edge length in cut  $a_p^{\text{lim}}$  varies with spindle speed.

## 2.2 Chatter in milling

Turning is usually a slow cutting process with a high tool tip resonance frequency which means that the number of vibration cycles during a full turn is large. This means that optimising a turning process with respect to chatter often given little room for improvement. The milling process is more prone to improvements from spindle speed optimisation and especially in the high speed machining segments. The main reason that the milling process can draw greater advantage from the stability optimisation is that the phase between the inner and outer surface modulations from one material removal cut is generated by two cutting teeth. Most of the commercial milling cutters have more than one cutting tooth resulting in a tooth passing frequency which is higher than the spindle revolution frequency. As a result of this, in combination with a more flexible cutting tool with lower resonance frequencies, a lower number of vibration waves  $N$  needs to be considered for normal spindle speeds. This results in larger and wider stability lobes, see Figure 3. The difference between "good" and "bad" spindle speeds is therefore larger in terms of stable cutting edge length in cut  $a_p$ , or axial depth of cut which is the proper term in milling.

### 2.2.1 Stability lobe diagrams in milling

The chatter phenomenon in milling has many similarities to the related phenomenon in turning but there are some differences, both in terms of chatter mechanics and stability theory. The most significant difference between milling and turning is that in the milling process the cutting tool is rotating and not the work piece as it is in turning. This makes the theoretical assessment of stability lobe analysis somewhat more cumbersome, since the cutting forces change both direction and amplitude during the cut. This is due to the change in orientation of the cutting tooth and variation in chip thickness, see Figure 4.

An analytical approach to the chatter stability diagram in milling was first derived by Budak and Altintas [3,4] who proposed a similar linearisation approach to the cutting force model as described in [1] and [2]. However, they included both the tangential and radial cutting forces,  $F_{t,m}$  and  $F_{r,m}$ , acting on the cutting tooth during cut.

For the  $m$ :th tooth we have

$$F_{t,m}(t) = k_t a_p h_m(t) \quad (10)$$

$$F_{r,m}(t) = k_r a_p h_m(t) \quad (11)$$

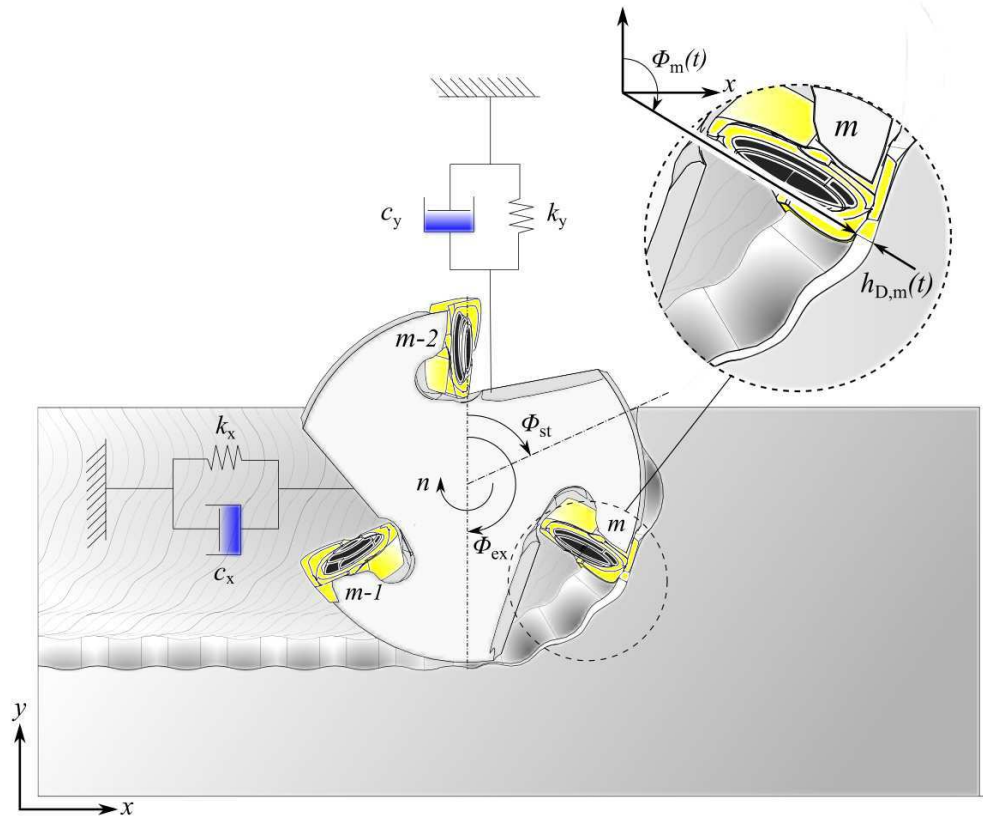


Figure 4: Illustration of a 2-DOF dynamic milling model considering transversal motion in two directions. The figure defines the entering angle  $\phi_{st}$ , and exiting angle  $\phi_{ex}$  in relation to the cutter and work piece. The dynamic chip thickness  $h_{D,m}(t)$ , is defined as the relation between the angle in cut  $\phi_m$ , of tooth  $m$  and the dynamic displacement between the two consecutive teeth  $m - 1$  and  $m$ .

The angle dependent chip thickness  $h_{D,m}(t)$ , see Figure 4, can be approximated as

$$h_{D,m}(t) = \begin{cases} f_z \sin \phi_m(t) + (v_{m-1} - v_m), & \phi_{st} < \phi_m < \phi_{ex} \\ 0, & \phi_{ex} < \phi_m < \phi_{st} \end{cases} \quad (12)$$

where  $f_z \sin \phi_m(t)$  is the static chip thickness and  $v_m$  and  $v_{m-1}$  is the dynamic displacements in radial direction of the  $m$ :th and  $(m - 1)$ :th cutting teeth. Equation (12) can be expressed as a function of the tooth passing period  $\tau$ , see Figure 5, as

$$h_{D,m}(t) = \begin{cases} f_z \sin \phi_m(t) + (v(t) - v(t - \tau)), & \phi_{st} < \phi_m < \phi_{ex} \\ 0, & \phi_{ex} < \phi_m < \phi_{st} \end{cases} \quad (13)$$

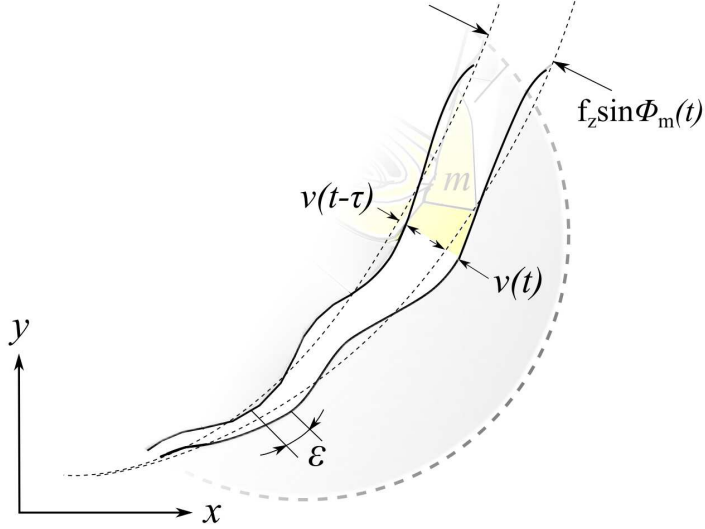


Figure 5: Illustration of the dynamic chip thickness in milling as a function of the static feed dependent chip thickness  $f_z \sin \phi_m(t)$ . Here  $f_z$  is the feed per tooth and  $\phi_m$  is the angle in cut. It is also a function of the phase shift  $\epsilon$ , which depend on the dynamic radial displacements  $v(t)$  and  $v(t - \tau)$ .

With the assumption that there is no coupling between the radial and tangential degrees of freedom the total force contribution from all cutting edges  $z$ , can be written as

$$F_x(t) = - \sum_{m=0}^{z-1} F_{t,m}(t) \cos \phi_m(t) - \sum_{m=0}^{z-1} F_{r,m}(t) \sin \phi_m(t) \quad (14)$$

$$F_y(t) = \sum_{m=0}^{z-1} F_{t,m}(t) \sin \phi_m(t) - \sum_{m=0}^{z-1} F_{r,m}(t) \cos \phi_m(t) \quad (15)$$

Here, the tangential and radial cutting forces have been projected to the table fixed coordinate system  $xy$ , see Figure 4.

Equations (14) and (15) were used in [3] and [4] to derive equations (16) and (17) as the foundation for the analytical stability lobe diagram of a milling process. These are for the axial depth of cut

$$a_p^{\text{lim}} = - \frac{2\pi \Re(\lambda)}{z k_t} (1 - \kappa) \quad (16)$$

where  $\lambda$  and  $\kappa$  can be found from

$$\lambda = -\frac{1}{2\alpha_0}\alpha_1 \pm \sqrt{\alpha_1 - 4\alpha_0}$$

with

$$\alpha_0 = H_{xx}(j\omega)H_{yy}(j\omega)(\alpha_{xx}\alpha_{yy} - \alpha_{xy}\alpha_{yx})$$

$$H_{xx}(j\omega) = \frac{1}{-\omega^2 M + j\omega c_x + k_x}$$

$$H_{yy}(j\omega) = \frac{1}{-\omega^2 M + j\omega c_y + k_y}$$

$$\alpha_1 = \alpha_{xx}H_{xx}(j\omega) + \alpha_{yy}H_{yy}(j\omega)$$

$$\alpha_{xx} = \frac{1}{2} \left[ \cos 2\phi - 2\frac{k_r}{k_t}\phi + \frac{k_r}{k_t} \sin 2\phi \right]_{\phi_{st}}^{\phi_{ex}}$$

$$\alpha_{xy} = \frac{1}{2} \left[ -\sin 2\phi - 2\phi + \frac{k_r}{k_t} \cos 2\phi \right]_{\phi_{st}}^{\phi_{ex}}$$

$$\alpha_{yx} = \frac{1}{2} \left[ -\sin 2\phi + 2\phi + \frac{k_r}{k_t} \cos 2\phi \right]_{\phi_{st}}^{\phi_{ex}}$$

$$\alpha_{yy} = \frac{1}{2} \left[ -\cos 2\phi - 2\frac{k_r}{k_t}\phi - \frac{k_r}{k_t} \sin 2\phi \right]_{\phi_{st}}^{\phi_{ex}}$$

$$\kappa = \frac{\Im(\lambda)}{\Re(\lambda)}$$

and the corresponding spindle speed is

$$n = \frac{60\omega}{z(\epsilon + 2\pi N)} \quad (17)$$

where the phase angle  $\epsilon$  is

$$\epsilon = \pi - 2\psi$$

and

$$\psi = \begin{cases} -\tan^{-1} \left| \frac{\Im H(j\omega)}{\Re H(j\omega)} \right| & \text{if } \Re H(j\omega) > 0, \Im H(j\omega) < 0 \\ -\pi + \tan^{-1} \left| \frac{\Im H(j\omega)}{\Re H(j\omega)} \right| & \text{if } \Re H(j\omega) < 0, \Im H(j\omega) < 0 \\ -\pi - \tan^{-1} \left| \frac{\Im H(j\omega)}{\Re H(j\omega)} \right| & \text{if } \Re H(j\omega) < 0, \Im H(j\omega) > 0 \\ -2\pi + \tan^{-1} \left| \frac{\Im H(j\omega)}{\Re H(j\omega)} \right| & \text{if } \Re H(j\omega) > 0, \Im H(j\omega) > 0 \end{cases}$$

### 2.3 Time domain chatter stability boundary

The analytical chatter stability methods for obtaining stability lobe charts has both advantages and disadvantages. One great advantage is that the analytical methods are fast. The two main phenomena the analytical methods does not consider are when the cutting tooth jumps out of the work piece due to excessive vibrations, and when the cutting force is strongly non-linearly related to feed or cutting speed. In these cases time domain simulations produce better results. The time domain simulation approach to predict chatter has been utilised by a number of researchers, see [5–14]. The two most commonly used methods for time domain chatter stability predictions are the Temporal Finite Element Analysis (TFEA) method, see [5, 6], and the Semi-Discretisation (SD) method, see [7–10].

The TFEA method compares the exact analytical solution for free tool vibration with an approximated solution of the tool vibrations during cut. The time-delay differential equation has no closed form solution for the milling process so an approximated solution of the tool in cut is therefore established by dividing the time in cut into finite numbers of elements for the comparison. The two systems are then compared in a discrete linear map where the stability is determined by the characteristic multiplier of the map.

The SD method has been employed to approximate the delay differential equations (DDE) describing the stability of milling and turning operations by a series of ordinary differential equations (ODE). This is achieved by approximating the time delay terms as piecewise constant functions.

The TFEA and SD methods have both been employed to predict stability lobe charts for a low radial immersion SDOF milling operation by Bayly *et. al.* and Insperger *et. al.* see [5] and [7]. Both methods were later extended to a more general 2 DOF milling operation by Mann *et. al.* [6] who used TFEA and Gradišek [11] which used the SD method. The various time domain methods, see [5–14], all have in common that they differ from the analytical methods in

that they have to be solved iteratively in order to find the stability boundary of the axial depth of cut  $a_p^{\text{lim}}$ . Common to all investigations presented in [5–14], is also that they all search for the bifurcation point, *i.e.* the limiting depth of cut where the system becomes unstable. Different bifurcation types has been found to occur with Hopf-bifurcation being the most common type. This usually manifests itself as a chatter frequency close to a natural frequency of the system, see [8]. The second bifurcation type observed using the TFEA method or the SD method is Flip-bifurcation which is characterised by a chatter frequency at harmonics of odd multiples of half the tooth passing frequency, see [11]. The time-domain solutions of milling and turning provides more information regarding the cutting process than the analytical methods. The time-domain simulation approach to the metal cutting process can be extended not only to determine chatter but also to quantify the severity of the vibrations and be used to predict surface texture during stable and unstable conditions, see [16].

### 3 Machining dynamics by component synthesis

Stability analysis for increased productivity and process reliability is used within the metal machining industry. However, the use is to some extent limited due to a number of factors. The methodology to employ the stability lobe analysis requires very experienced users to conduct the measurements of system transfer functions and to carry out the stability analysis. The use of the methodology is also affected by the requirements on the measurement procedure. To obtain the correct dynamic flexibility at the tool tip for a specific cutting tool it is required that the cutting tool is mounted in the machine tool of interest at test time. The use of a test rig or a FE representation of the machine tool have been proven insufficient in order to obtain the correct damping and stiffness parameters of a machine tool. This is mainly due to the mechanical joint complexity of the machine tool structure. Furthermore the test procedure requires that the machine tool has to be still standing during measurement. This results in loss of valuable production time. The productivity loss during measurements of a machine tool mounted cutting tools can be expensive for larger production plants. Large production facilities can be equipped with more than 30 machine tools where each machine tool may carry a substantial amount of cutting tools due to the modularity of today's tooling concepts, see Figure 6.

In an effort to reduce measurement time a number of researchers, see [17–25], have utilised component synthesis to obtain the dynamic flexibility of a machine tool mounted cutting tool. The approach to the problem is to regarding the cutting tool and the machine tool as two separate subsystems and then employed component synthesis to construct the FRFs of transversal motion at the tool

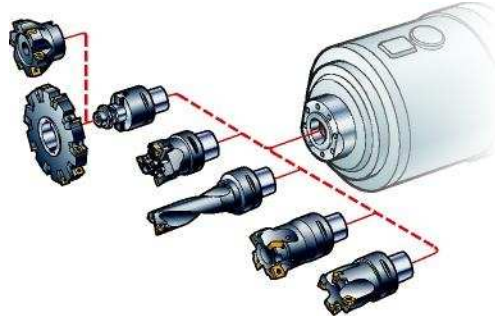


Figure 6: Machine tool modularity. This figure shows seven cutting tools but a magazine of a machine tool can hold up to over 100 cutting tools.

tip which are required for the stability lobe prediction. Dividing the machine tool/cutting tool assembly into subcomponents allows any system identification to be conducted on subsystem level. This means that the measurements of the machine tool dynamics only has to be conducted once. The system description of the cutting tool, which is a less complex mechanical component, can be a FE representation of the tool.

The substructuring approach to predict the tool tip dynamics were first taken by Schmitz and Donaldson [17] who coupled an analytically obtained subsystem representation of the free-free cutting tool to FRFs of the machine tool/tool holder assembly. These FRF:s were estimated from impact test data. The coupling was made on the measured machine tool subcomponent FRFs to the analytically obtained FRFs of the free-free cutting tool substructure directly. This methodology require that the measurements has low noise contamination, see section 4.2 for details. In their work, the rotational degree of freedoms (RDOFs) were neglected in the experimental characterisation of the coupling between the machine tool/tool holder subassembly. An interface flexibility between the two subassemblies were instead introduced to compensate for the neglected RDOFs. The introduction of the interface flexibility required an additional measurement of representative machine tool/tool holder mounted cutting tool to calibrate the interface flexibility properties. Their work were extended to include the RDOFs reported in [18]. However, these theoretical extensions were not validated due to the absence of reliable measurement techniques of the FRFs. The problem to obtain the RDOFs at the tool connection point on the machine tool substructure was addressed in [19]. A measurement procedure was proposed that allowed the RDOFs to be obtained by measurements conducted on two blank calibration cylinders. The proposed procedure was to conduct impact testing on one short blank cylinder and one longer cylinder and then calculate the

RDOFs based on these measurements. The cutting tool FRFs at the connection point were then constructed using a FE-model of a cylindrical beam. An alternative approach to retrieve the RDOFs at the connection point between machine tool side of the substructures were taken by Schmitz and Duncan [21]. The methodology they proposed included a triple-component coupling strategy where the machine tool and the base geometry of a tool holder were considered as one substructure. The tip of the tool holder with the inserted part of the cutting tool constituted another substructure and the part of the cutting tool outside of the tool holder was the third substructure. To obtain the RDOFs about the connection point between the machine tool and tool holder base and the tip of the tool holder they proposed a two step method. This consists of a first step in which measurements of the translational DOFs at the free end of a machine tool mounted representative tool holder were conducted. Then the RDOFs were calculated based on a receptance decoupling method, were the part of the general tool holder from the base to the tip were subtracted. From these the machine tool/tool holder base receptances could be obtained. A filtering method applied to the measurements of the machine tool/tool holder was also suggested to minimise the noise influence. An emphasis on the advantage of using Timoshenko beam models rather than Euler-Bernoulli beam models to represent the cutting tool substructure were made in Erturk *et. al.* in [22]. The advantage with the Timoshenko representation over the Euler-Bernoulli is that the rotary inertia and especially the shear deformation is considered. This is important for accurately calculate the eigenvalues for cutting tools with small length to diameter ratio, for details see [26]. A study on the implication of noise contaminated measurements on coupling of machine tool/cutting tools were conducted By Schmitz and Duncan [23]. The concluding remarks from this study were that the noise contamination may strongly influence the results due to the matrix inversion made during the coupling of the FRFs. Park and Chae [24] further developed the approach taken by Schmitz and Donaldson in [19] in which the transfer function associated to the RDOFs were retrieved based on measurements conducted on calibration gauge cylinders. The novelty presented in [24] was the use of a flexible joint similar to the approach taken in [17]. In [24] it was showed that this approach further could enhance the accuracy of the model of the coupled system. An alternative approach to the flexible joint approach presented in [24] were taken by Mancisidor *et. al.* [25] who also used the methodology presented in [19] to retrieve the RDOFs but, modelled the cutting tool as a clamped-free component and thereby obtained the fixed boundary behaviour of the cutting tool. By utilising this approach the modes needed to be considered of the cutting tool component could be lowered significantly with the same level of model accuracy.

## 4 Component synthesis theory

Modelling of complex dynamic structures may sometimes be cumbersome. Access limitations to do proper instrumentation of physical components or unknown joint dynamic properties in a FEM representation of a structure, are some examples of problems that may be encountered. In these cases it is sometimes better to model the complete structure by component synthesis of substructures. This methodology divides the structure into subcomponent which each is modelled separately. This enables a more versatile modelling approach where a mixture of experimentally and analytically obtained dynamic models of each subcomponent can be combined to synthesise the complete system. A variety of subsystem synthesis methods stand at disposal with different benefits and drawbacks. These methods has traditionally been divided in to two main categories, direct frequency response function (FRF) based coupling and component mode synthesis (CMS).

### 4.1 Component mode synthesis

Component mode synthesis is usually employed to couple models set up from physical first-principle laws such as FE models. The two most commonly used strategies by CMS, couples the subcomponents by either the fixed-interface or free-interface mode method. The utilisation of the fixed-interface mode method employing CMS were first conducted by Hurty [27] in the mid 1960s. The method he developed was later simplified by Craig and Bampton [28] which, instead of imposing that each interface DOF separately were required to be rigid-body freedoms and redundant interface freedoms, regarded the interface DOFs together. This made the method more accurate and more computationally efficient. The adjustments they made, made the method more suitable for finite element (FE) implementation and it is today widely used within this field of simulations. The free-interface mode method was first introduced by Craig and Bampton in [29] which considered the component modes to be vibrating modes with free interface DOFs. The free-interface mode approach has also been taken by Rixen [30] providing a coupling method called Dual Craig-Bampton method which preserved the sparsity of the mass and stiffness matrices exhibited by the residual-flexibility matrix in lieu to the method developed in [29]. The method developed by [30] proved to be more accurate than the Craig-Bampton method in terms of the estimating eigenfrequencies of the coupled system. A more thorough survey of the different CMS methodology's and theories can be found in the book by Craig and Kurdila [31].

## 4.2 FRF based coupling

This methodology is a coupled model synthesis based on frequency response models of each subcomponent. The frequency response models can be obtained either from synthesised modal models or from measured FRFs directly. The ability to use measured FRFs is one of the most distinguishing features of the FRF based coupling method compared to CMS. Modal analysis errors can hereby be eliminated and contribution of high frequency modes can be accounted for since this information is embedded within the measured data. The fundamental idea of FRF based coupling originated by impedance coupling method (IC-method) which describes the boundary DOFs at the joints between substructures by impedance matrices.

### 4.2.1 Impedance coupling method

With this method the information of kinematic constraints and equilibrium conditions is carried through the impedance matrix  $\mathbf{Z}(\omega)$ . It was first derived by Bishop and Johnson in [32]. They describe the force and displacement continuity through the coupling points between the assembled subsystems. The impedance matrix can be both frequency dependent and complex-valued and describes generalised force vectors  $\{f\}$  in terms of generalised response vectors  $\{q\}$  such that

$$[\mathbf{Z}(\omega)] \{q\} = \{f\} \quad (18)$$

However, generalised response vectors in terms of generalised force vectors is usually described by the receptance matrix  $\mathbf{H}(\omega)$  of the system.

$$\{q\} = \mathbf{H}(\omega) \{f\} \quad (19)$$

From Equation (18) and Equation (19) we note that the receptance matrix  $\mathbf{H}(\omega)$  is the inverse of the impedance matrix  $\mathbf{Z}(\omega)$

$$\mathbf{H}(\omega) = \mathbf{Z}(\omega)^{-1} \quad (20)$$

From Equation (20) one can see that problems with the inversion of  $\mathbf{H}$  occurs when the matrix is not square, which is often the case when receptance is obtained from measurements.

To utilise the impedance matrix in coupling of substructures it is needed to implement compatibility and equilibrium conditions, see Figure 7. The generalised response co-ordinate of the assembled structure,  $q_c$ , has to be coincident with the coupling co-ordinates of the substructures to be assembled such that

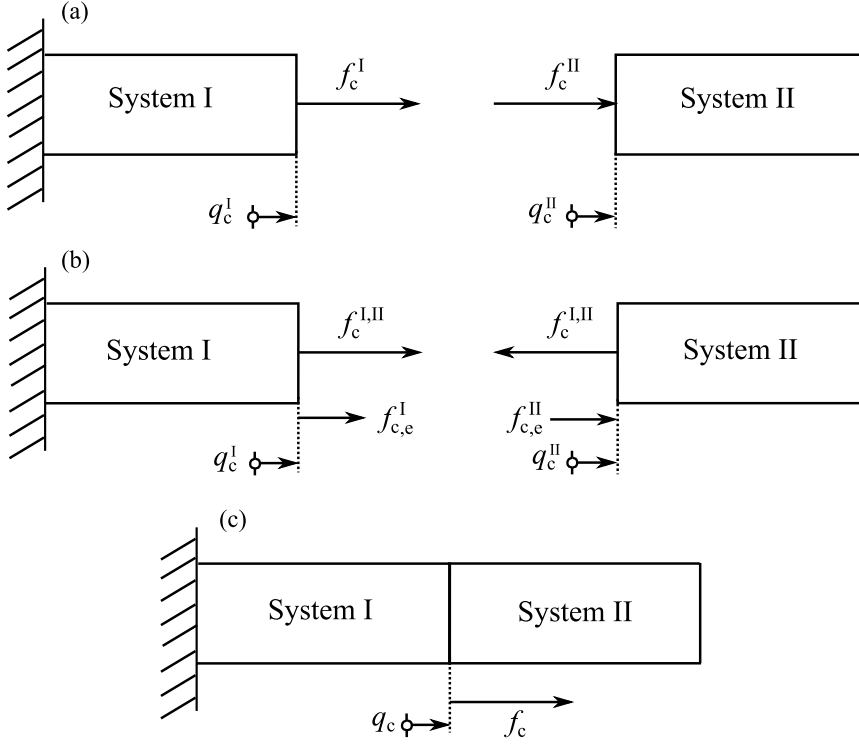


Figure 7: Illustration of coupling procedure. (a) Uncoupled subsystems I and II. (b) Kinematic and equilibrium constraints introduced. (c) Coupled system I+II

$q_c \stackrel{def}{=} q_c^I = q_c^{II}$  and the total external load applied to the interface DOFs of the assembly has to fulfil the requirement that  $f_c \stackrel{def}{=} f_c^I + f_c^{II} = f_c^{I,II} + f_{c,e}^I - f_c^{I,II} + f_{c,e}^{II} = f_{c,e}^I + f_{c,e}^{II}$  where  $f_c^{I,II}$  denotes the cross-sectional force between the two components and  $f_{c,e}$  is the externally applied force to the interface DOFs.

These conditions can be written in matrix form with use of the transformation matrix  $\mathbf{T}$ , for details see [33], as

$$\{q_s\} = [\mathbf{T}] \{q_c\} \quad (21a)$$

$$\{f_c\} = [\mathbf{T}]^T \{f_s\} \quad (21b)$$

Where subscript  $s$  refers to the co-ordinates on the substructure. If we write Equation (18) as an matrix equation of subsystems

$$[\mathbf{Z}_s(\omega)] \{q_s\} = \{f_s\} \quad (22)$$

and utilising the compatibility and equilibrium conditions in Equation (21) we can rewrite Equation (22) as

$$\{q_c\} = \left( [\mathbf{T}]^T [\mathbf{Z}_s(\omega)] [\mathbf{T}] \right)^{-1} \{f_c\} \quad (23)$$

From Equation (23) we can see that the receptance matrix of the assembled system  $\mathbf{H}(\omega)$  corresponds to

$$\mathbf{H}(\omega) = \left( [\mathbf{T}]^T [\mathbf{Z}_s(\omega)] [\mathbf{T}] \right)^{-1} \quad (24)$$

This methodology fulfils all physical requirements needed through the compatibility and equilibrium conditions but it is numerically inefficient. The method requires two matrix inversions. First of the subsystem receptance matrix  $\mathbf{H}_s(\omega)$  to obtain the impedance matrix  $\mathbf{Z}_s(\omega)$  and then a full size matrix inversion of Equation (24). The inversion of the matrices makes this method especially sensitive to measurement noise and matrix rank deficiencies which may cause significant errors in the coupled model. The notation of  $\mathbf{H}(\omega)$  and  $\mathbf{Z}(\omega)$  will subsequently be changed to  $\mathbf{H}$  and  $\mathbf{Z}$  for brevity. It is however still implied that  $\mathbf{H}$  and  $\mathbf{Z}$  are frequency dependent.

#### 4.2.2 Generalised FRF impedance coupling technique

An alternative method to the IC-method were developed by Jetmundsen *et. al.* in [34]. The number of required matrix inversions were reduced to one. This methodology applied to coupling of two subcomponents, I and II, provides us with the following matrix equation

$$\mathbf{H} = \begin{bmatrix} \mathbf{H}_{cc}^I & \mathbf{H}_{co}^I & 0 \\ \mathbf{H}_{oc}^I & \mathbf{H}_{oc}^I & 0 \\ 0 & 0 & \mathbf{H}_{oo}^{II} \end{bmatrix} - \begin{bmatrix} \mathbf{H}_{cc}^I \\ \mathbf{H}_{oc}^I \\ -\mathbf{H}_{oc}^{II} \end{bmatrix} \left( \mathbf{H}_{cc}^I + \mathbf{H}_{cc}^{II} \right)^{-1} \begin{bmatrix} \mathbf{H}_{cc}^I \\ \mathbf{H}_{oc}^I \\ -\mathbf{H}_{oc}^{II} \end{bmatrix}^T \quad (25)$$

where  $\mathbf{H}$  is the synthesised assembled receptance matrix and subscript (c) and (o) denotes interface and other DOFs respectively. A more general derivation of Equation (25) were conducted by Ren and Beards in [33] to further utilise the concept of graph theory and mapping matrices, presented in [34] and [35] for the boolean operation of an arbitrary number of substructures.

### 4.3 State-space based coupling

The substructure synthesis method used to couple subcomponents both in **Paper A** and **Paper B**, has been the state-space based coupling technique proposed by Sjövall [36]. The state-space based coupling methodology is closely related to FRF based coupling in that identical kinematic and equilibrium constraints are enforced on the coupling. The state-space method approach to couple substructures were first taken by Su and Juang in [37] arguing several advantages compared to FRF-based coupling method. Some of the more prominent advantages enlightened by [37] were avoidance of ill-conditioned matrix inversions of the FRF matrices and simplicity in identification on subsystem level with the estimation of several lower order models. This is made rather than estimating a higher order model on coupled system level. The state-space based coupling method proposed by [36] distinguishes from [37] in that [36] applies proper similarity transformations of the subsystem state-space models in lieu to [37] that instead proposed introduction of two additional auxiliary state variables to each interface DOF. The method is described in fuller detail in **Paper B**.

## 5 Summary of appended papers

In **Paper A**, *Dynamic substructuring in metal cutting machine chatter*, the conceptual approach of the chosen EMA and system identification methodology was applied to a physical test rig. The state-space coupling algorithms were employed to couple the identified test rig structure to a synthesised subsystem representing the cutting tool based on the mass and inertia properties retrieved from a CAD model of the cutting tool. The simplification of the cutting tool subsystem were based on the assumption that such approximation should be valid for the relatively short and rigid tool tip selected for investigation. The synthesised FRFs of the assembled substructures were compared and evaluated against measurements of the fully assembled test rig.

In **Paper B**, *Experimental-analytical substructure model sensitivity analysis for cutting machine chatter prediction*, a sensitivity analysis of parameter influence on the coupled system were conducted. A number of parameters related to the identification process were perturbed in order to see the magnitude of influence each parameter had on the coupled system. The effect of perturbation of parameters such as state-order, FRF response magnitude, damping estimation and cut of frequency were investigated. A reference systems were constructed based on an FE-model of the test rig used in **Paper A** and the parameter influence investigation were conducted based on perturbations of the reference

system.

## 6 Conclusions and future work

The application and implementation of the coupling methodology on the physical test rig presented in **Paper A** gave encouraging results. However, it could be concluded that the stability lobe predictions seemed sensitive to small deviations between the synthesised model and reference measurements of the fully assembled system. The parameter sensitivity analysis conducted in **Paper B** indicated that exceptional care must be taken during measurements of the machine tool subcomponent and that sufficient state order is of the essence. The conclusions drawn from **Paper A** and **Paper B** is that the coupling methodology using state-space formulation seems very promising from which several advantages can be utilised compared to other coupling methods. However, a more robust measurement procedure has to be developed before the coupling and measurement methodology is applied on to a machine tool. This concludes that more work on the measurement method has to be conducted on the test rig set up before moving on to a real machine tool.

## References

- [1] J. Thustly and M. Polacek. The stability of machine tools against self excited vibrations in machining. *International Research in Production Engineering*, ASME:465–474, 1963.
- [2] S. A. Tobias. *Machine Tool Vibrations*. Blackie and Sons Ltd., 1965.
- [3] E. Budak and Y. Altintas. Analytical prediction of chatter stability in milling—part i: General formulation. *Journal of Dynamic Systems, Measurement, and Control*, 120(1):22–30, 1998.
- [4] E. Budak and Y. Altintas. Analytical prediction of chatter stability in milling—part ii: Application of the general formulation to common milling systems. *Journal of Dynamic Systems, Measurement, and Control*, 120(1):31–36, 1998.
- [5] P.V. Bayly, B.P. Mann, T. L. Schmitz, D. A. Peters, S. Gabor and T. In-sperger. Effects of radial immersion and cutting direction on chatter instability in end-milling. In *Proceedings of IMECE 2002, ASME International Mechanical Engineering Congress and Exposition, New Orleans, Louisiana, 2002*.

- [6] B.P. Mann, P.V. Bayly, M.A. Davies, and J.E. Halley. Limit cycles, bifurcations, and accuracy of the milling process. *Journal of Sound and Vibration*, 277(1-2):31 – 48, 2004.
- [7] T. Insperger, B.P. Mann, G. Stépán, and P.V. Bayly. Stability of up-milling and down-milling, part 1: alternative analytical methods. *International Journal of Machine Tools and Manufacture*, 43(1):25 – 34, 2003.
- [8] T. Kalmár-Nagy, S. Gábor, and F. Moon. Subcritical hopf bifurcation in the delay equation model for machine tool vibrations. *Nonlinear Dynamics*, 26:121–142, 2001.
- [9] T. Insperger, D.A.W. Barton, and G. Stépán. Criticality of hopf bifurcation in state-dependent delay model of turning processes. *International Journal of Non-Linear Mechanics*, 43(2):140 – 149, 2008.
- [10] T. Insperger and G. Stépán. Chatter suppression of turning process via periodic modulation of the spindle speed - a 1 dof analysis. In *Proceedings of the Third Conference on Mechanical Engineering, Budapest, Hungary*, 2002.
- [11] J. Gradišek, M. Kalveram, T. Insperger, K. Weinert, G. Stépán, E. Govkar, and I. Grabec. On stability prediction for milling. *International Journal of Machine Tools and Manufacture*, 45(7–8):769 – 781, 2005.
- [12] M.X. Zhao and B. Balachandran. Dynamics and stability of milling process. *International Journal of Solids and Structures*, 38(10-13):2233 – 2248, 2001.
- [13] J. Gradišek, E. Govkar, and I. Grabec. Chatter onset in non-regenerative cutting: A numerical study. *Journal of Sound and Vibration*, 242(5):829 – 838, 2001.
- [14] A. Ganguli. *Chatter reduction through active vibration damping*. PhD thesis, Université Libre De Bruxelles, Bruxelles, Belgium, 2005.
- [15] Y. Altintas. *Manufacturing Automation: Metal Cutting Mechanics, Machine Tool Vibrations and CNC Design*. Cambridge University Press, 2000.
- [16] K. Weinert, T. Surmann, D. Enk, and O. Webber. The effect of runout on the milling tool vibration and surface quality. *Production Engineering*, 1:265–270, 2007.
- [17] T.L. Schmitz and R.R. Donalson. Predicting high-speed machining dynamics by substructure analysis. *CIRP Annals - Manufacturing Technology*, 49(1):303 – 308, 2000.

- [18] T. L. Schmitz, Matthew A. D., and Michael D. K. Tool point frequency response prediction for high-speed machining by RCSA. *Journal of Manufacturing Science and Engineering*, 123(4):700–707, 2001.
- [19] S. S. Park, Y. Altintas, and M. Movahhedy. Receptance coupling for end mills. *International Journal of Machine Tools and Manufacture*, 43(9):889 – 896, 2003.
- [20] T. Schmitz. Receptance coupling for high-speed machining dynamics prediction. *Proceedings of the 21st International Modal Analysis Conference*, pages 1–12, 2003.
- [21] T. L. Schmitz and G. S. Duncan. Three-Component Receptance Coupling Substructure Analysis for Tool Point Dynamics Prediction. *Journal of Manufacturing Science and Engineering*, 127(4):781, 2005.
- [22] A. Erturk, H. Ozguven, and E. Budak. Analytical modeling of spindle – tool dynamics on machine tools using Timoshenko beam model and receptance coupling for the prediction of tool point FRF. *International Journal of Machine Tools and Manufacture*, 46(15):1901–1912, 2006.
- [23] T. Schmitz and G. Duncan. Receptance coupling for dynamics prediction of assemblies with coincident neutral axes. *Journal of Sound and Vibration*, 289(4-5):1045–1065, 2006.
- [24] S. S. Park and J. Chae. Joint identification of modular tools using a novel receptance coupling method. *The International Journal of Advanced Manufacturing Technology*, 35(11-12):1251–1262, 2008.
- [25] I. Mancisidor, M. Zatarain, J. Muñoa, and Z. Dombovari. Fixed Boundaries Receptance Coupling Substructure Analysis for Tool Point Dynamics Prediction. *Advanced Materials Research*, 223:622–631, 2011.
- [26] S. Timoshenko, D. H. Young, and W. Weaver. *Vibration Problems in Engineering*, volume 208. John Wiley and Sons, Inc., 1990.
- [27] W. C. Hurty. Dynamic analysis of structural systems using component modes. *AIAA Journal*, 3(4):678–685, 1965.
- [28] R.R. Craig, Jr. and M. C. C. Bampton. Coupling of substructures for dynamic analysis. *AIAA Journal*, 6(7):1313–1319, 1968.
- [29] R.R. Craig, Jr. and M. C. C. Bampton. On the use of attachment modes in substructure coupling for dynamic analysis. In *AIAA/ASME 18th Structures, Structural Dynamics and Materials Conference, San Diego, CA*, 1977.

- [30] D. J. Rixen. A dual Craig-Bampton method for dynamic substructuring. *Journal of Computational and Applied Mathematics*, 168(1-2):383–391, 2004.
- [31] R.R. Craig, Jr. and A. J. Kurdila. *Fundamentals of Structural Dynamics*. John Wiley & Sons, Hoboken, New Jersey, 2006.
- [32] R. E. D. Bishop and D. C. Johnson. *The mechanics of vibration*. Cambridge University Press, Cambridge, 1960.
- [33] Y. Ren and C.F. Beards. On substructure synthesis with frf data. *Journal of Sound and Vibration*, 185(5):845–866, 1995.
- [34] B. Jetmundsen, R. L. Bielawa and W.G. Flannelly. Generalized frequency domain substructure synthesis. *Journal of the American Helicopter Society*, 33(1):55–64, 1988.
- [35] B. Jetmundsen. *On frequency domain methodologies for prescribed structural modification and subsystem synthesis*. PhD thesis, Rensselaer Polytechnic Institute, Troy, New York, 1986.
- [36] P. Sjövall. *Identification and Synthesis of Components for Vibration Transfer Path Analysis*. PhD thesis, Chalmers University of Technology, Gothenburg, Sweden, 2007.
- [37] T. J. Su and J. N. Juang. Substructure system identification and synthesis. *Journal of Guidance, Control and Dynamics*, 17(5):1087–1095, 1994.

**Part II**  
**Appended papers A-B**



---

# Paper A

## Dynamic substructuring in metal cutting machine chatter



# Dynamic substructuring in metal cutting machine chatter

**A. Liljerehn<sup>1</sup>, A. Johansson<sup>2</sup>, T. Abrahamsson<sup>2</sup>**

1 AB Sandvik Coromant, R and D Metal Cutting Research  
SE-811 81 Sandviken, Sweden  
email: [anders.c.liljerehn@sandvik.com](mailto:anders.c.liljerehn@sandvik.com)

2 Chalmers University of Technology, Department of Applied Mechanics  
SE-412 96, Gothenburg, Sweden

## Abstract

In metal cutting, spindle speed optimisation for process stability is one example of action that may reduce production time and increase process reliability. For process stability, it is crucial to avoid regenerative vibrations and thereby enable larger cutting depth, with higher material removal rate as benefit. A spindle speed optimisation is usually based on the machine tool and cutting tool assembly's frequency response at the tool-tip. This is normally obtained by dynamic testing of the full assembly. In this paper we use a receptance coupling technique to reduce testing time by synthesising the frequency response displacement function of the system. The method utilises test data of the machine tool with an inserted blank tool together with a finite element representation of the real cutting tool. The coupling is made via a state space coupling technique. Comparisons are made with data from full system tests and a stability prediction is demonstrated.

## 1 Introduction

The industry for making metal cutting tools has traditionally been product oriented. As a result of this, a long time standing development focus has been towards product evolution of standard tool families such as face or shoulder milling cutters, parting or grooving tools for turning, and indexable tools for drilling. Cutting tool manufacturers have now started to intensify their focus

on services and application niches for their products in order to add more value to the tool customers and widen the market. Spindle speed optimisation with respect to process stability is one example of application service that can be provided. For this, it is crucial to avoid regenerative vibrations, or so-called chatter, a well-known phenomenon in metal cutting that ruins the surface finish and may damage the cutting tool. Spindle speed optimisation with respect to chatter has been a vast research area since the mid 1950's. Early researchers such as [1] and [2] derived linear analytical expressions for prediction of chatter stability. Their method relied on a linearisation of the excitation force from the cutting process, which permitted Laplace domain equations of stability to be derived. A further development of the analytical stability equation was introduced by [3], who introduced a dynamic milling model with directional dynamic milling force coefficients, thereby enabling an analytical solution of the milling stability problem. The assumption that the cutting process is linear is unfortunately often far from true. Phenomena like non-linear process damping, non-linearities in spindle bearings and the non-linear relation between cutting force and chip thickness are some examples that may influence the stability of the cutting process. Time domain analysis of stability is one way of permitting non-linearities to enter into the governing equations, but is often time consuming to conduct. One of the corner-stones when obtaining a stability chart is the Frequency Response Function (FRF) at the tip of the machine tool mounted cutter. The most frequently used FRFs are the transfer functions from applied point loads to displacement responses. These FRFs are usually obtained through tap tests. Two problems are associated with the FRF measurements. Firstly, the machine tool has to be still standing which means that valuable production time will be lost. Secondly, the resulting FRF is only valid for the particular tool set-up being tested. A machine tool with a plenitude of cutting tools in its tool magazine then requires a very time consuming measurement process. One way of reducing the measurement time is to use a receptance coupling technique to calculate the FRF at the tool tip instead of measuring it. This approach allows the frequency response to be obtained from substructure synthesis from a mixture of subsystem characterisations based on measurements or mathematical modelling. Modelling of a machine tool structure is hard because of its mechanical complexity, and its description is therefore preferably obtained through system identification from measured data. The considerably simpler cutting tool components can be modelled by finite elements, sometimes with Timoshenko beam elements [4]. As pointed out in [4], the quality of the FRF obtained from receptance coupling is strongly influenced by the ability to identify the dynamics at the point of connection of each substructure. In the case of system identification based on vibration testing of the machine tool structure, high quality measurements are of the essence. The limited space

---

and time available to conduct measurements in a machine tool in production almost always excludes the use of sophisticated test set-ups, such as using shakers as a source of excitation. Limited space for sensor placement can also be a problem when it comes to measuring the multi-dimensional motion required to capture the dynamics at the coupling joint. Attempts to exclude direct measurements of rotational degrees of freedom have been made in [4] and [5]. In [5], all rotational degrees of freedom were excluded from the coupling joint and replaced by a spring and damper connection between the machine tool - tool holder - tool assemblies. The stiffness and damping coefficients were then calibrated so that the assembled receptance coupled system and measurements matched. This approach may however be problematic when the connection stiffness changes between the holder and the tool at different insertions. In the work of [4], the rotational degrees of freedom were instead calculated from cross FRFs obtained from measurements on a blank tool with a protrusion. In this work we use differentiation of translational motion of physically separated sensors to obtain rotations. We use a dynamic component synthesis technique for the system modelling. As a method of component synthesis we use a scheme of state-space model coupling [6]. We use a mixture of white-box and black-box state-space models for component description. The white-box components are established using validated finite element system matrices to obtain the corresponding state-space models. In our application, these are used to represent the tool component, which normally is not too complex for an accurate finite element representation. The black-box components rely on state-space models obtained from system identification based on vibration test data. However, also complementary physical insight is used to constrain the system identification and hence the resulting model might be considered as a grey-box model. The importance of physically motivated constraints is emphasised in [6]. Known physical properties, such as stability properties, reciprocity properties, passivity properties and modal density properties are accounted for. These properties originate from observations that are independent of the vibration test. In our application, we use grey-box modelling for the cutting machine, for which the cost of obtaining a validated finite element model may be prohibitive. The subsystem state-space models are transformed to a coupling form, at which kinematic constraints and equilibrium conditions for the component interfaces are imposed. The procedure is applied to a test rig, in which the cutting tool is fitted to a simplified physical model of a cutting machine. Particular care is taken to obtain the proper model order of the grey box model of the cutting machine to suit the frequency range from 20 Hz to 2.5 kHz. The quality of the obtained FRF from state-space model synthesis, used for stability prediction, is very much dependent on the ability to determine the correct model order of the experimentally determined components, [6]. We compare predicted and mea-

sured coupling point FRFs and their corresponding stability lobes to validate the procedure.

## 2 Component synthesis

Techniques for coupling of experimentally determined models are traditionally based either on using measured FRFs directly [4, 7–10] or via modal synthesis [11–14]. The latter being an approach which is challenging in the respect that accurate mode shapes and sometimes even fixed interface mode shapes are needed. This demands a detailed spatial resolution in the measurements and, at times, extra measurements for fixed interface modes, see further overviews in [15] and [16]. The former methodology is more common, arguing simplicity and completeness. This is in the sense that the response in the frequency domain of interest is accurately represented by the unaffected FRFs, while modal regularisation truncates the effects of higher frequency modes. However, the modal regularisation ensures intelligible results while FRF coupling often suffers from numerical ill-conditioning and high noise sensitivity due to necessary matrix inversions.

In an effort to avoid the adverse effects of both methods, we have elected to use a method by [6]. This uses a coupling technique based on an identified first-order state-space model in lieu of a second-order modal model. This poses less severe restrictions on the model and less demands on the measurements while still regularising the data, see [17]. The method couples two subsystems ( $i = 1, 2$ ) represented by state-space models with external force inputs  $\mathbf{u}$  and displacement outputs  $\mathbf{y}$

$$\begin{cases} \dot{\mathbf{x}}^i = \mathbf{A}^i \mathbf{x}^i + \mathbf{B}^i \mathbf{u}^i \\ \mathbf{y}^i = \mathbf{C}^i \mathbf{x}^i \end{cases} \quad (1)$$

The state vector is  $\mathbf{x}$ , and  $\mathbf{A}$ ,  $\mathbf{B}$  and  $\mathbf{C}$  are constant coefficient matrices. Both subsystems are partitioned with respect to coupling degrees of freedom (DOFs), subscript c, and other DOFs, subscript o, according to the partition of response and loading

$$\mathbf{y}^i = \begin{Bmatrix} \mathbf{y}_c^i \\ \mathbf{y}_o^i \end{Bmatrix}, \quad \mathbf{u}^i = \begin{Bmatrix} \mathbf{u}_c^i \\ \mathbf{u}_o^i \end{Bmatrix} \quad (2)$$

Using the non-uniqueness of state-space representations, the system might be transformed with no loss of accuracy. A similarity transform  $\mathbf{T}$  with certain properties transforms the states as

$$\tilde{\mathbf{x}}^i = \mathbf{T}^i \mathbf{x}^i = \begin{Bmatrix} \dot{\mathbf{y}}_c^i \\ \mathbf{y}_c^i \\ \mathbf{x}_o^i \end{Bmatrix} \quad (3)$$

It can be shown, see [6], that the state-space matrices in this case turn into the particular coupling form as

$$\tilde{\mathbf{A}}^i = \begin{bmatrix} \mathbf{A}_{vv}^i & \mathbf{A}_{vd}^i & \mathbf{A}_{vo}^i \\ \mathbf{I} & 0 & 0 \\ 0 & \mathbf{A}_{od}^i & \mathbf{A}_{oo}^i \end{bmatrix}, \quad \tilde{\mathbf{B}}^i = \begin{bmatrix} \mathbf{B}_{vv}^i & \mathbf{B}_{vo}^i \\ 0 & 0 \\ 0 & \mathbf{B}_{oo}^i \end{bmatrix}, \quad (4)$$

$$\tilde{\mathbf{C}}^i = \begin{bmatrix} 0 & \mathbf{I} & 0 \\ \mathbf{C}_{ov}^i & \mathbf{C}_{od}^i & \mathbf{B}_{oo}^i \end{bmatrix}$$

The partition subscripts indicate velocity outputs ( $v$ ), displacement outputs ( $d$ ) and other states ( $o$ ), all in accordance with Equation 3. At this stage coupling the models together is merely an exercise in using equilibrium and compatibility conditions, see further [6].

In [6], it is proven that systems of the form seen in Equation 1 can be taken to the coupling form of Equation 4, provided that there is no direct throughput term for velocity responses from applied forces at the coupling DOFs, requiring that  $\mathbf{C}^i \mathbf{B}^i = 0$ . Since Newton's second law relates forces to accelerations directly, and velocities need to be integrated from accelerations, in theory this is a valid assumption.

### 3 The FE models

Besides being modelled from test data as described later, the test rig (henceforth called substructure I, see Figure 1), was also modelled with finite elements. This was made for validation of the receptance coupling technique. In this validation procedure, the results of the state-space coupling of components both modelled by finite elements were compared with results of a finite element analysis of the system modelled as a single entity.

The finite element model of the tool tip (henceforth called substructure II, see Figure 2) is based on material property data and data from a CAD specification of its geometry. A real tool tip was weighed on a scale to validate the model's mass properties. The second order finite element model representation was taken to a first-order state space form to suit the state-space coupling procedure.

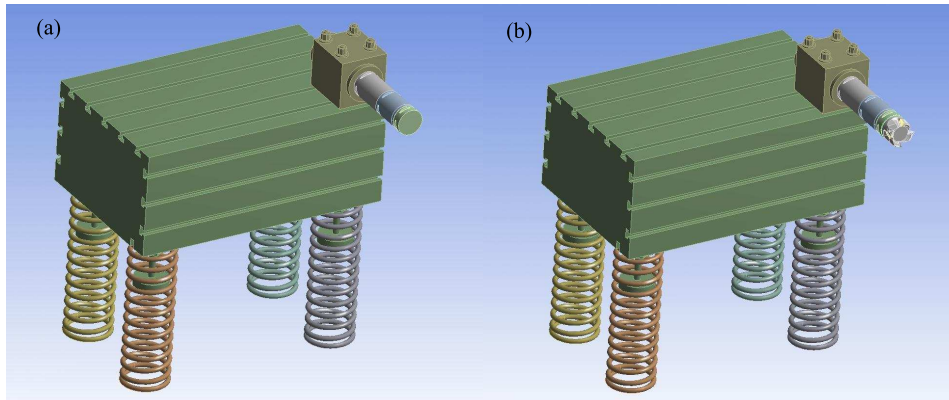


Figure 1: Figure (a) shows test rig with blank tool. Figure (b) shows test rig with tool. The helical springs were modelled as massless linear springs. The main body, the fixture and other components were modelled with flexible brick elements.

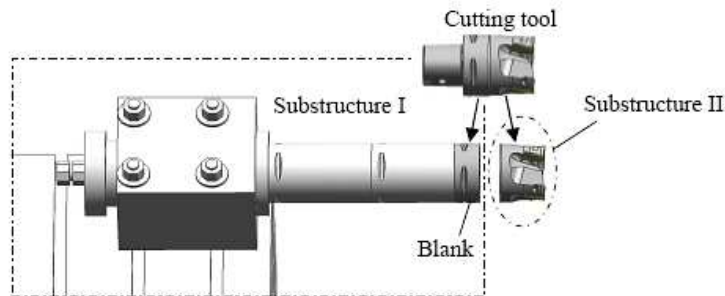


Figure 2: Substructures I (part of) and II

### 3.1 Validation of the substructuring method

A validation of the receptance coupling method was made by coupling of state-space component models of substructures I and II. A truncated modal representation using the modal solution from a finite element analysis was used for substructure I. Substructure II is very short and stiff and it was concluded that a rigid body representation was sufficient for that part. The eigenvalues were calculated for the coupled state-space system and compared with the eigenvalues of the FEM representation of the assembled system. The eigenvalues of both solutions are given in Table 1. The comparison shows a good correlation up to about 2 kHz which validates the coupling method. Above 2 kHz it is believed that the deviations originate from the simplified representations of the tool tip (substructure II) and interfacing surfaces.

Table 1: Eigenfrequencies of finite element analysis and from the eigensolution of the receptance coupled state-space model.

Mode nr	FE Model	Identified model
1	0.5	0.5
2	0.6	0.5
3	1.0	0.9
4	1.2	1.2
5	1.8	1.6
6	2.1	1.9
7	216.4	216.4
8	217.3	217.3
9	217.8	217.8
10	218.1	218.1
11	218.6	218.6
12	219.4	219.4
13	220.0	220.0
14	221.7	221.7
15	363.4	363.4
16	364.0	364.0
17	364.2	364.1
18	370.1	370.1
19	425.9	426.2
20	432.0	432.3
21	1217.3	1217.7
22	1399.8	1400.2
23	1582.7	1582.7
24	1592.8	1592.7
25	1604.4	1604.4
26	1606.8	1606.8
27	1619.2	1619.2
28	1638.0	1638.0
29	1643.0	1643.0
30	1648.1	1647.9
31	1725.1	1725.7
32	1948.0	1949.2
33	2169.7	2176.0
34	2351.1	2370.2
35	2365.8	2381.6

## 4 Test set-up and measurement procedure

A test was performed for method evaluation using a sprung test rig as a substitute for a machine tool, see Figure 3. The rationale for not using a real machine tool is that the real machine tool spindle often shows a non-linear behaviour, which introduces an unwanted degree of complexity at this stage of our research. The cutting tool set-up consists of a fixture containing Coromant Capto C8 coupling with a draw bar fitted with two distance extensions, (Sandvik Coromant article code C8-391.01-80 100 and C8-391.01-80 125). Tests were conducted using one set-up with a blank tool and another set-up with a milling tool, see Figure 3.

The test rig with the fixture, the two extensions and only a smaller part of the cutting tool R790-084C8S1- H22, here referred to as the blank, constitutes subsystem I, see Figure 2. The blank shares the same geometric base as the CoroMill 790 tool containing the Coromant Capto C8 coupling and the gripping groves but lacks the tip with the flutes and inserts. The tip constitutes subsystem II, see Figure 2. All cutting tools with integrated machine tool spindle coupling of this type have the same geometric base. However, the complete tool geometry can vary with different overhang, diameter and number of inserts. The use of a blank tool has two major advantages. The first is that the surface of the blank facing the tool tip is very stiff. This makes the end surface remain almost planar also for high-frequency vibrational modes, requiring few degrees-of-freedom for representing the surface motion. This is crucial since this surface constitutes the interfacing surface to subsystem II, the tool tip. The use of the blank also permits easy placement of the accelerometers

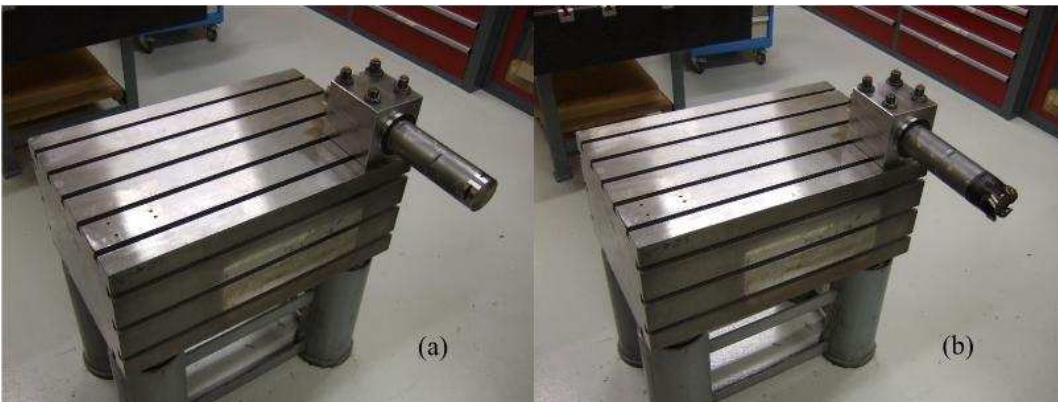


Figure 3: Test rig used for experimental modal analysis. Picture (a) shows set-up with blank and picture (b) shows set-up with milling tool.

at the interface surface, which permits rotational acceleration estimation from measured translational accelerations.

An experimental characterisation was made for subsystem I, requiring decisions regarding placement of sensors and method of external dynamic loading. The chosen sensor set-up consisted of eight accelerometers. Four of the accelerometers were placed at the end face of the blank, while the remaining four were placed at a distance of 60 mm from the end of the blank measuring in radial direction, with 90 degree spacing between each, see Figure 4a. A shaker was used as excitation source. The excitation points were at the face of the blank and at the distance of 60 mm from the end of the blank, see Figure 4a.

Measurements with the cutting tool mounted at the end of the extension instead of the blank are required to evaluate the receptance coupling results. These tests were conducted in the same way as with the blank with the exception that the accelerometers mounted on the front face of the blank were positioned at the face of the tool instead. The sensor positions on the test rig with tool can be viewed in Figure 4b.

The tests were made using a stepped sine procedure to obtain FRF by use of regression analysis. Care was taken to obtain stationary conditions at each frequency step and also to provide a balanced excitation level to avoid strong non-linearity but still to maintain a good signal-to-noise ratio. We used multiple SIMO test set-ups in which we kept the position of the accelerometers but moved the single shaker to three different positions, see Figure 4. The frequency range covered by the test was from 20 Hz to 4.5 kHz in 0.25 Hz increments.

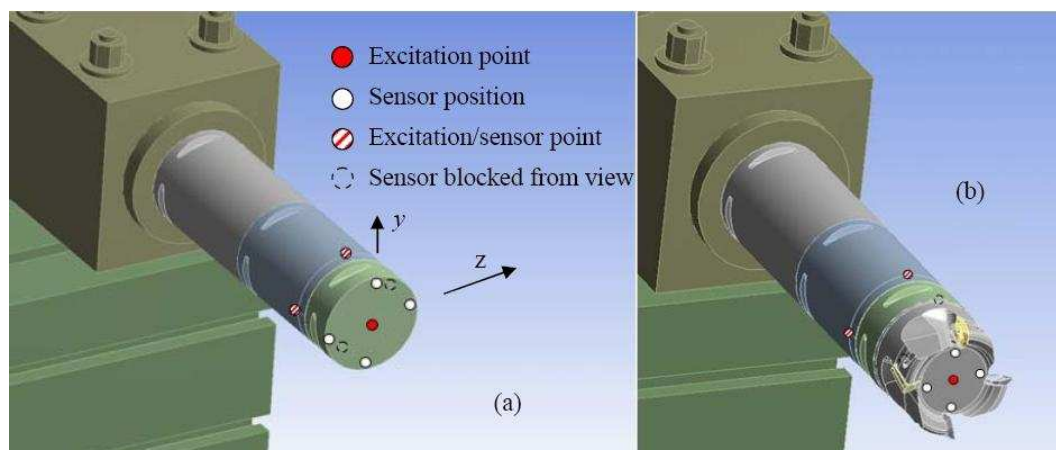


Figure 4: Test rig used for experimental modal analysis. Picture (a) shows set-up with blank and picture (b) shows set-up with milling tool.

However, a non-optimal shaker configuration gave low-quality results in the upper frequency range. Linear accelerometers were used in a configuration that allowed for calculation of rotational accelerations about the transversal axes of the blank by the use of differentiation. No registration of rotations about the longitudinal axis of the tool was made since it was considered insignificant for chatter stability analysis. Examples of recorded frequency response functions can be seen in Figure 5. It may be noted that full reciprocity for cross transfer functions was not obtained, see Figures 5b and 5c. This was probably due to imperfections in the test set-up, such as cross sensitivities of accelerometers and that excitation forces and measured accelerations were not perfectly collinear.

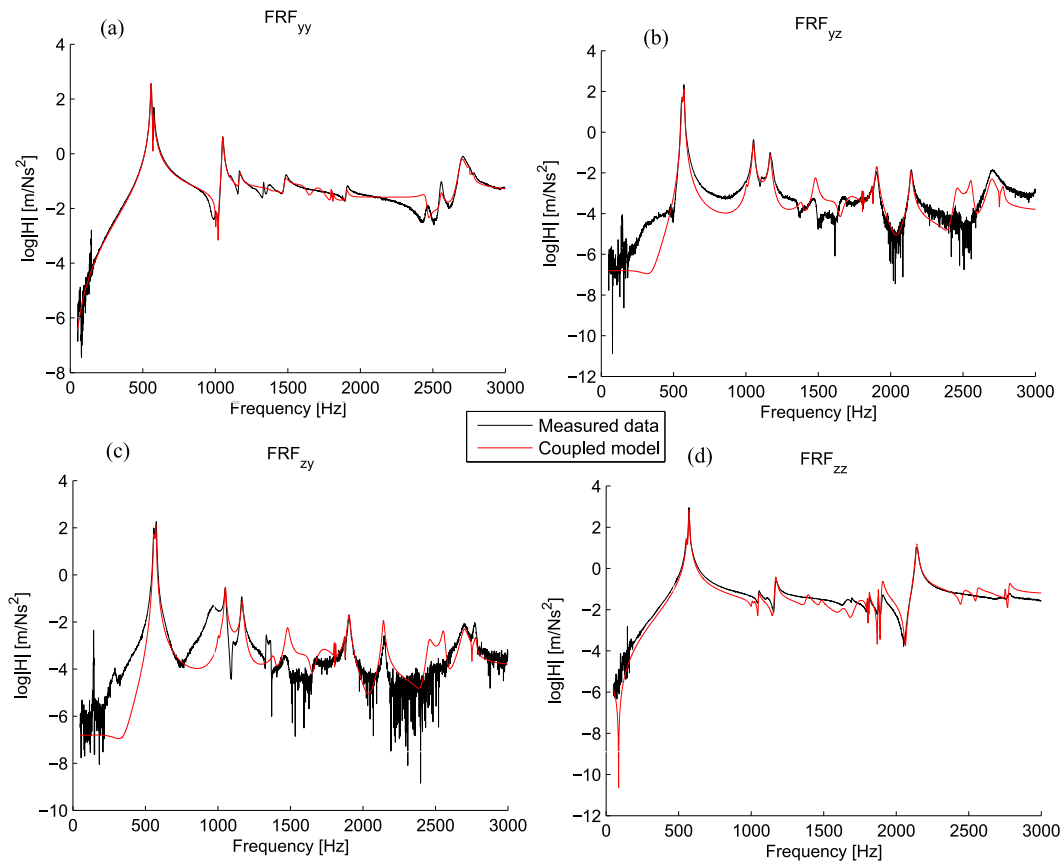


Figure 5: Measurements and system identification results.

## 5 System identification

The state-space sub-space method N4SID (see [20]), as implemented in the System Identification Toolbox for Matlab, was used for system identification. This method identifies the parameters of a first-order state space model of the form

$$\begin{cases} \dot{\mathbf{x}} = \mathbf{A}\mathbf{x} + \mathbf{B}\mathbf{u} \\ \mathbf{y} = \mathbf{C}\mathbf{x} + \mathbf{D}\mathbf{u} \end{cases} \quad (5)$$

Here  $\mathbf{u}$  and  $\mathbf{y}$  are the system input and output vectors, respectively,  $\mathbf{A}$ ,  $\mathbf{B}$ ,  $\mathbf{C}$  and  $\mathbf{D}$  are the state-space coefficient matrices and  $\mathbf{x}$  is the state vector, see further [18]. The identified model to be used in the subsequent coupling method is highly dependent on the use of the proper number of states, see [6]. The number of states is not identified by the method but needs to be specified by the user of the method.

A scheme of sequential identifications elaborated on later in this chapter was used in lieu of direct application of N4SID, since more model states than physically motivated were needed to get best fit to test data in a direct application. It should be noted that physical infeasibility of models identified directly with N4SID can largely be deduced to measurement errors, such as system poles being variant to relocation of shakers and sensors between test sets. In short: When we change positions of sensors and actuators, we are implicitly assuming that our system remains unaffected when in fact it is unavoidably altered by changes in the measurement system, see also [19]. That this was the reason for some of the unintuitive pole placements stemming from the direct application of N4SID to MIMO data was also verified through SISO studies of two direct FRFs. For example, pole location stability charts verified that each direct FRF contained only two poles in the frequency range 500 - 600Hz<sup>1</sup> although direct application of N4SID indicated substantially more poles.

Since the first and second bending modes of the distance extensions at the tool are of major importance for chatter stability, an initial identification of the system matrices was made by using lateral directional accelerance FRFs only. In these modes, the extension motion is largely perpendicular to the longitudinal axis. This procedure was also motivated by issues with reciprocity and noise levels in the measurements (see Chapter 3). Using accelerance FRFs had two distinct benefits over using receptances or mobilities, the signal-to-noise ratio was kept high, and the average amplitude level was mainly the same over the entire frequency range of the test.

## 5.1 Sequential identification

It was stated previously that the coupling routine is sensitive to the model order used in identification, and that due to small set-up changes in the measurements, more states than physically motivated were required to obtain identified models with good fit to experimental data. To address the first issue while circumventing the second, we began by identifying a high order model that gave a good fit over the entire frequency range of interest, from 400 Hz to 3 kHz. This was used as a baseline model. It was verified that the residual, retrieved when subtracting FRFs synthesised using this model from the measurement FRFs, is several orders of magnitude lower than measurement data. Ideally, the residual should be inseparable from the flat spectrum of white noise, which it was not in reality.

Next, the frequency range was separated into eight intervals, each containing a reasonably well defined number of modes. This is not unlike the separate weighing of frequency bands reported in [20]. Using a diagonalising similarity transform of the baseline model, for each of the eight intervals, the test data was cleared from poles outside the frequency range of current interest in a frequency domain filtering procedure, and system identification was performed on the band-limited FRFs

$$\bar{\mathbf{H}}(\omega) = \mathbf{H}_M(\omega) - \mathbf{H}_{synt}(\omega) \quad (6)$$

Here  $\mathbf{H}_M(\omega)$  is the measurement FRF matrix and  $\mathbf{H}_{synt}(\omega)$  is the FRF matrix synthesised from the baseline model cleared from poles in the frequency interval. A model of a reasonable order was identified for each frequency interval. The order selected was based on insight given by complementary FE analyses and physical reasoning. Finally the state-space models obtained for the separate frequency ranges were coupled in parallel to yield a model of an order credible.

In order to improve the model's low frequency asymptote, six low-frequency modes of the FE solution (see Chapter 4) were added to the model. Also, one high-frequency residual state outside of the frequency range of the test was included to improve the behaviour at the high end of the frequency range.

Finally, the full  $\mathbf{B}$ ,  $\mathbf{C}$  and  $\mathbf{D}$  matrices of Equation 5 were estimated from all measured data available, thus including the longitudinal translation as well as the rotations about the transversal axes. A method using non-linear least-squares fitting was used for this estimation, see [21].

## 5.2 Reciprocity

Non-gyroscopic, non-circulatory and passive mechanical systems, such as the present, are expected to obey Betti's reciprocity principle. Yet the measured cross-FRFs are not fully consistent with this. As stated previously, this is probably due to measurement shortcomings. However, it follows that the identified model is not reciprocal, i.e. it is not self-adjoint. To impose model reciprocity, a modal method was used. By solving the eigenvalue problem for the right eigenvectors of  $\mathbf{A}$  in equation 5 and assuming selfadjointness, a modal based state-space model is established, in a manner similar to that of [22]. After this step, the identified model is further expanded to include input at the rotational DOFs using modal synthesis.

At this stage, the model is set up for displacement output. A model with displacement output should satisfy the relations

$$\mathbf{D} = 0, \quad \mathbf{CB} = 0 \quad (7)$$

since a model with velocity output should have no direct throughput. This feature is used in the coupling algorithm, see Chapter 2. It was found that by introducing a number of spurious poles, the extended state space model could be made consistent with these relations with only a minor influence of the system transfer functions. Direct FRFs for the lateral directions, deemed most important to the coupling, are shown in Figure 6.

Note that the two modifications described in this section both deteriorate the identified model's overall correlation with measured data. They are introduced to ensure a degree of physical feasibility which is needed for successful component synthesis. An alternative *modus operandi* would have been to use an identification method tailored for the specific application, such as [23], thereby ensuring these properties from the start.

## 6 Chatter stability prediction

To describe the theory of chatter stability prediction is beyond the scope of this paper. However, the final target of our efforts is to be able to predict instability based upon the established FRFs. We have been using standard chatter prediction methods, see [24], to establish stability lobes based on synthesised FRFs of the compound system and FRFs obtained from a vibration test of the assembled system. We used cutting parameters given in Table 2 for the stability analysis. The resulting stability lobes are seen in Figure 7.

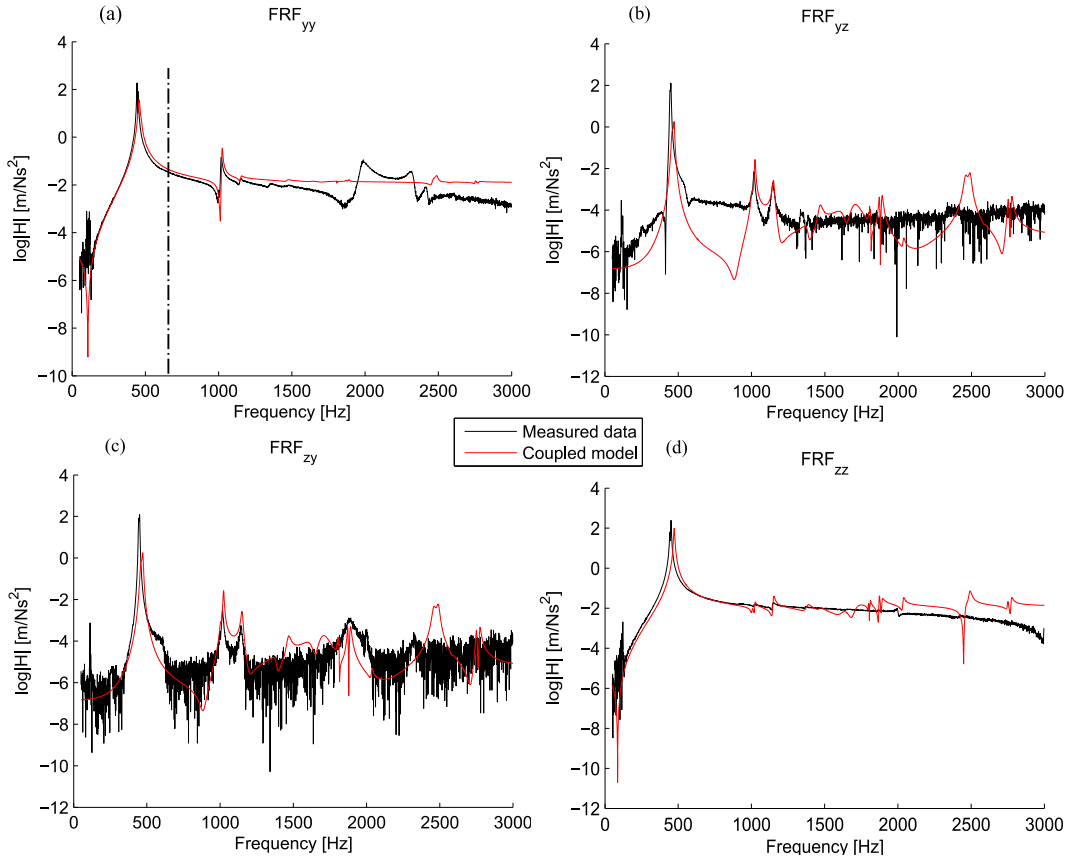


Figure 6: Synthesised FRFs after system coupling compared with measured data. The broken vertical line in Figure 6a indicates the eigenvalue of the first bending mode of subsystem I located at 558 Hz. After coupling the location of the eigenvalue of the first bending mode in  $FRF_{yy}$  was 458 Hz for the synthesised system and 443 Hz in the measured fully assembled test rig.

Table 2: Cutting parameters used in simulation of stability lobes

Cutting parameters	Quantity	Unit
Number of teeth, $z$	6	—
Tool diameter, $D_c$	80	[mm]
Radial width of cut, $a_e$	80	[mm]
Cutting force coefficient in tangential direction, $K_t$	1319	[MPa]
Cutting force coefficient in radial direction, $K_r$	789	[MPa]

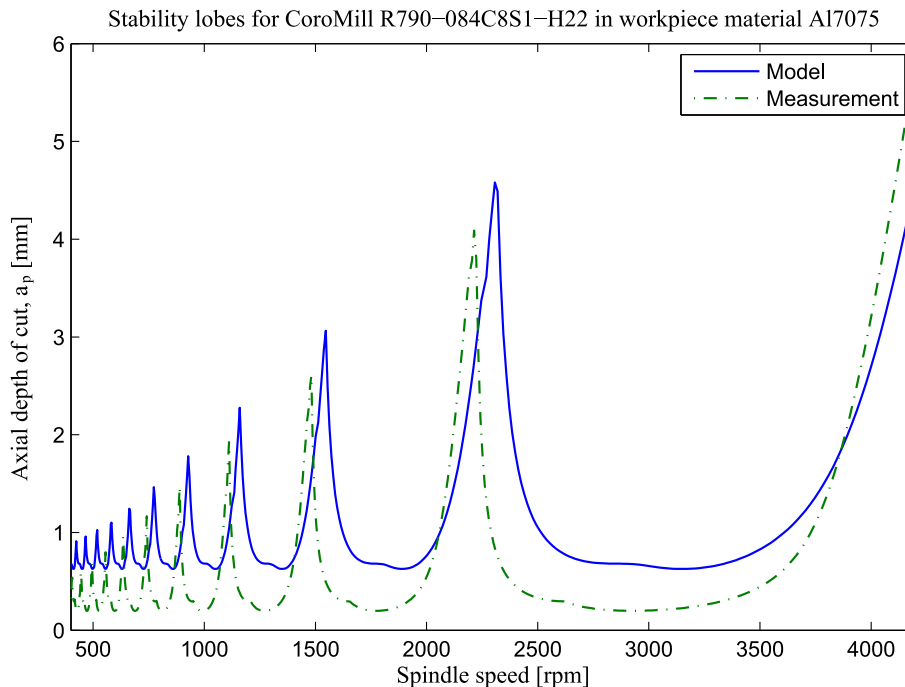


Figure 7: Stability lobes based on FRF's directly from measurement and from the synthesised model. Stable cutting operation conditions are obtained below the curves. The curves determine the onset of instability.

The stability lobes are found to be predominantly characterised by the first pair of bending modes of the extensions which occurs at about 460 Hz. While challenging measurement situations and subsequent system identification have caused us to over-estimate their frequencies by a few Hertz, throwing the stability lobes off, the major part of the frequency shift caused by adding the tool tip (Substructure II), about 100 Hz, has been successfully captured by the method; an encouraging result.

## 7 Discussion and Conclusion

This article investigates the possibility of modelling a machine tool set-up using dynamic component synthesis with the ultimate objective to lay the foundation for chatter stability analysis. This should be made possible to use for an entire tool family while performing but one set of measurements, on a generic tool stub referred to as the blank.

The methodology has been implemented on a test rig equipped in turn with both blank and tool, with encouraging results. However, it is found that small deviations in the system identification of the tool-and blank measurements at the first bending mode of the identified model propagates and increases into the coupled model. The coupling method is also found to be sensitive to the selected order of the identified model, in line with the findings of [6].

A deviation of more than a few Hertz of the vibrational frequency of the first bending modes of the coupled system has been found sufficient for shifting the stability lobes, making significant impact on stability predictions. Hence, high quality measurements and precision system identification seems essential for the method to work well. Since machine tool magazines can hold hundreds of tools, and the alternative is to measure each machine-and-tool assembly separately, time spent here may still prove economical.

In the course of work, sensitivity analyses with respect to a multitude of parameters including geometrical properties of the joint, frequency and residue of the first bending mode of the identified machine tool and blank model as well as its model order have been carried out, and different modulus operandi for enforcing reciprocity and direct velocity throughput considerations have been tested. We intend to continue such analyses.

## References

- [1] J. Tlustly and M. Polacek. The stability of machine tools against self excited vibrations in machining. *International Research in Production Engineering*, ASME:465–474, 1963.
- [2] S. A. Tobias. *Machine Tool Vibrations*. Blackie and Sons Ltd., 1965.
- [3] E. Budak and Y. Altintas. Analytical prediction of chatter stability in milling—part i: General formulation. *Journal of Dynamic Systems, Measurement, and Control*, 120(1):22–30, 1998.
- [4] S. S. Park, Y. Altintas, and M. Movahhedy. Receptance coupling for end mills. *International Journal of Machine Tools and Manufacture*, 43(9):889 – 896, 2003.
- [5] T. L. Schmitz, Matthew A. D., and Michael D. K. Tool point frequency response prediction for high-speed machining by RCSA. *Journal of Manufacturing Science and Engineering*, 123(4):700–707, 2001.

- 
- [6] P. Sjövall and T. Abrahamsson. Component system identification and state-space model synthesis. *Mechanical Systems and Signal Processing*, 21(7):2697–2714, 2007.
- [7] R. L. Bielawa J. H. Gordis and W. G. Flannelly. A General Theory for Frequency Domain Structural Synthesis, *Journal of Sound and Vibration*. *Journal of Sound and Vibration*, 150(1):139–158, 1998.
- [8] W. Liu and D. J. Ewins. Substructure synthesis via elastic media. *Journal of Sound and Vibration*, 257(2):361–379, 2002.
- [9] T. Lim. A Theoretical and Computational Study of the FRF-Based Substructuring Technique Applying Enhanced Least Square and Tsvd Approaches. *Journal of Sound and Vibration*, 231(4):1135–1157, 2000.
- [10] Y. Ren and C.F. Beards. On substructure synthesis with frf data. *Journal of Sound and Vibration*, 185(5):845–866, 1995.
- [11] R. R. Craig and M. C. C. Bampton. Coupling of Substructures for Dynamic Analyses. *AIAA Journal*, 6(7):1313–1319, 1968.
- [12] D. J. Rixen. A dual Craig-Bampton method for dynamic substructuring. *Journal of Computational and Applied Mathematics*, 168(1-2):383–391, 2004.
- [13] C. W. Jen, D. A. Johnson, and F. Dubois. Numerical modal analysis of structures based on a revised substructure synthesis approach. *Journal of Sound and Vibration*, 180(2):185–203, 1995.
- [14] E. Balmes. Use of generalized interface degrees of freedom in component mode synthesis. In *International Modal Analysis Conference IMAC. SEM*, Bethel, CT, USA, 1996.
- [15] L. Meirovitch. *Computational methods in structural dynamics*, volume 49. Springer, 1980.
- [16] R.R. Craig, Jr. and A. J. Kurdila. *Fundamentals of Structural Dynamics*. John Wiley & Sons, Hoboken, New Jersey, 2006.
- [17] T. J. Su and J. N. Juang. Substructure system identification and synthesis. *journal of Guidance, Control and Dynamics*, 17(5):1087–1095, 1994.
- [18] L. Meirovitch. *Dynamics and Control of Structures*. Prentice Hall PTR, 1990.

- [19] D. J. Ewins. *Modal Testing: Theory, Practice and Application*. Research studies press LDT., 2001.
- [20] T. McKelvey. Frequency Weighted Subspace Based System Identification in the Frequency Domain. In *Proceedings of the 34th IEEE Conference on Decision and Control*, volume 2, pages 1228–1233. IEEE, 1995.
- [21] L. Ljung. *System Identification: Theory for the User (2nd Edition)*. Prentice Hall PTR, 1998.
- [22] T. Abrahamsson. Modal-parameter extraction for nonproportionally damped linear structures, In *Proceedings of IMAC IV*, London, 1987.
- [23] P. Sjövall, T. McKelvey and T. Abrahamsson. Constrained State-Space System Identification with Application to Structural Dynamics. *Automatica*, 42:1539–1546, 2006.
- [24] Y. Altintas. *Manufacturing Automation: Metal Cutting Mechanics, Machine Tool Vibrations and CNC Design*. Cambridge University Press, 2000.

---

# Paper B

## Experimental-Analytical Substructure Model Sensitivity Analysis for Cutting Machine Chatter Prediction



### Experimental-Analytical Substructure Model Sensitivity Analysis for Cutting Machine Chatter Prediction

A. Liljerehn<sup>1</sup>, T. Abrahamsson<sup>2</sup>

1 AB Sandvik Coromant, R and D Metal Cutting Research  
SE-811 81 Sandviken, Sweden  
email: [anders.c.liljerehn@sandvik.com](mailto:anders.c.liljerehn@sandvik.com)

2 Chalmers University of Technology, Department of Applied Mechanics  
SE-412 96, Gothenburg, Sweden

### Abstract

Process reliability and dynamic stability is a growing customer demand in the metal machining industry. A limiting factor in process stability is regenerative vibrations which may damage the machined component, the cutting tool and even the machine tool. Spindle speed optimisation to ensure process stability and enable larger cutting depths is based on the machine tool and cutting tool assembly's frequency response at the tool-tip. The traditional procedure to retrieve the tool-tip frequency response is to conduct dynamic testing of each machine tool mounted cutting tool. This methodology is normally very time consuming. In an attempt to reduce testing time, receptance coupling substructure analysis (RCSA) has been proposed by a number of researchers. The objective with this approach is to measure the machine tool structure once and then couple a finite element based substructure representation of the cutting tool of interest. The accuracy of the predicted tool-tip frequency response is then dependent on the quality of measured data. This paper details the state-space based sub-structure coupling technique that is used and presents a sensitivity analysis. This analysis distinguishes key considerations for the machine tool component test and it quantifies the parameter influence on the process stability predictions of the coupled system.

# 1 Introduction

In metal cutting, spindle speed optimisation for process stability is one example of action that may reduce production time and increase process reliability. For process stability, it is crucial to avoid regenerative vibrations due to feedback of the cutting forces and thereby enable larger cutting depth, with higher material removal rate as benefit. An analytical spindle speed optimisation is based on the real part of frequency response functions, FRFs, in two orthogonal transversal directions at the tool tip of a machine tool and cutting tool assembly. Based on the real part of the tool tip FRFs, a chart of what is known as stability lobes can be constructed, see Figure 1. The stability lobe chart indicates optimal spindle speeds where regenerative vibrations can be avoided for larger depths of cut. The chart, Figure 1, should be read as follows. A stable machining process can be expected if the spindle speed and axial depth of cut is in a combined state in the stable region of the chart. In the unstable state, however, regenerative vibrations also known as chatter do occur. From the stability chart one can see that some spindle speeds are more optimal than others where greater cutting depths, and thus a better production, are allowed without encountering chatter. The stability chart is only constructed out of the negative values of the real part of FRF of two orthogonal main directions at the tool tip of the cutting tool. The construction of the whole set of stability lobes to create the complete stability chart is based on the phase shifts between the vibration marks left on the machined surface made from two following cutting teethe that comes into cut, see [1].

Stability lobe predictions have been a vast research area since the early 1960's, [2,3]. One of the limitations of FRF-based chatter predictions is that the FRF

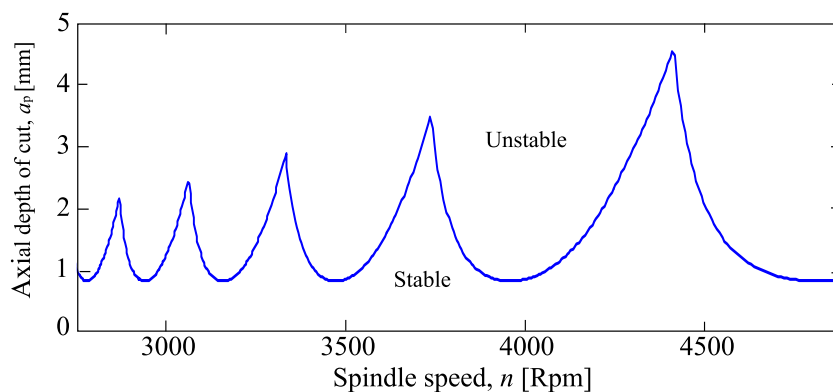


Figure 1: Stability lobe chart.

at the tool tip of a machine tool and cutting tool assembly only yields for a specific set-up. Larger production plants are usually equipped with a substantial amount of cutting tools in their machine tools. To measure each machine tool/cutting tool combination is not only time consuming but it also requires that the machine tool is taken out of operation during measurements. This results in productivity losses which in many cases are regarded as unacceptable by the plant company. To reduce testing time receptance coupling substructure analysis (RCSA) has been utilised by a number of researchers. The objective with this approach is to only measure the machine tool structure once and then couple a substructure representation of the cutting tool of interest into an assembly.

To use a receptance coupling technique by synthesising the frequency response displacement function of the system is indeed very appealing but is not without obstacles. This paper is a factor relevance investigation, trying to answer questions that aroused after the writing of [4]. One of the conclusions drawn in [4] was that a slight overestimation of the first bending mode of the coupled system's spindle/cutting tool assembly, compared to verification measurements, can have a large impact on the stability chart. The question of which parameters effects the result of the substructured system is one of the key understandings that need to be in place in order to conduct relevant measurements and stability lobe predictions. The factor relevance investigation in this paper is strictly restricted to FRFs generated from FEM of the assembly components. The models are described in [4] and the coupling routines used are fully described in [5]. The approach of using synthetic data has been chosen in order to avoid the complexity and uncertainties that follows with measurements in terms of noise, misalignment of force and output sensors, etc. The necessity of further sensitivity analyses to the measurement problem is evident.

## 2 Component synthesis

Component substructuring is usually divided into two main categories. The first is direct frequency response function coupling [6–11]. The direct FRF coupling method has the advantage that it is fast in that sense that it can be applied directly on measured FRFs and don't require a system identification data processing. The absence of data processing is also its biggest disadvantage since it makes this type of coupling techniques sensitive to noise. The other type of coupling methods often found in literature is component mode synthesis [12–15]. This method has the advantage that it diminishes the noise problems but on the other hand requires that the mode shapes are captured well and it may also suffer from errors that can come from mode truncation. The mode

truncation issue for the modal synthesis coupling technique is not a problem in the direct FRF coupling methods since the influences of higher frequency modes are accounted for in the measurement data. The component synthesis used in this sensitivity analysis is based on the state-space coupling method proposed in [5]. This coupling method utilises the benefits of noise suppression introduced by modal analysis. This is done by coupling of identified first-order state-space substructure component models. The coupling method is used to couple two subsystems ( $i = 1, 2$ ) on state-space form with displacement or velocities as output. A state-space model with external force inputs  $\mathbf{u}$  and displacement outputs  $\mathbf{y}$  can be written as follows

$$\begin{cases} \dot{\mathbf{x}}^i = \mathbf{A}^i \mathbf{x}^i + \mathbf{B}^i \mathbf{u}^i \\ \mathbf{y}^i = \mathbf{C}^i \mathbf{x}^i \end{cases} \quad (1)$$

The state vector is  $\mathbf{x}$ , and  $\mathbf{A}$ ,  $\mathbf{B}$  and  $\mathbf{C}$  are constant coefficient matrices. Both subsystems are partitioned with respect to coupling degrees of freedom (DOFs), subscript c, and other DOFs, subscript o, according to the partition of response and loading

$$\mathbf{y}^i = \begin{Bmatrix} \mathbf{y}_c^i \\ \mathbf{y}_o^i \end{Bmatrix}, \quad \mathbf{u}^i = \begin{Bmatrix} \mathbf{u}_c^i \\ \mathbf{u}_o^i \end{Bmatrix} \quad (2)$$

Using the non-uniqueness of state-space representations, the system might be transformed with similarity transformation without approximation. A similarity transform  $\mathbf{T}$  with certain properties transforms the states as

$$\tilde{\mathbf{x}}^i = \mathbf{T}^i \mathbf{x}^i = \begin{Bmatrix} \dot{\mathbf{y}}_c^i \\ \mathbf{y}_c^i \\ \mathbf{x}_o^i \end{Bmatrix} \quad (3)$$

it can be shown, see [5], that the state-space matrices in this case turn into the particular coupling form as

$$\tilde{\mathbf{A}}^i = \begin{bmatrix} \mathbf{A}_{vv}^i & \mathbf{A}_{vd}^i & \mathbf{A}_{vo}^i \\ \mathbf{I} & \mathbf{0} & \mathbf{0} \\ \mathbf{0} & \mathbf{A}_{od}^i & \mathbf{A}_{oo}^i \end{bmatrix}, \quad \tilde{\mathbf{B}}^i = \begin{bmatrix} \mathbf{B}_{vv}^i & \mathbf{B}_{vo}^i \\ \mathbf{0} & \mathbf{0} \\ \mathbf{0} & \mathbf{B}_{oo}^i \end{bmatrix}, \quad (4)$$

$$\tilde{\mathbf{C}}^i = \begin{bmatrix} \mathbf{0} & \mathbf{I} & \mathbf{0} \\ \mathbf{C}_{ov}^i & \mathbf{C}_{od}^i & \mathbf{C}_{oo}^i \end{bmatrix}$$

The partition subscripts indicate velocity outputs (v), displacement outputs (d) and other states (o), all in accordance with Equation (3). The next stage in order to couple the models together, equilibrium and compatibility conditions

has to be taken into account at the coupling DOFs. For response of two subsystems that are co-oriented and numbered in the same order we can write the relation between the response quantities and the uncoupled subsystem models and the synthesised models as

$$\begin{Bmatrix} \mathbf{y}_c^I \\ \mathbf{y}_c^{II} \end{Bmatrix} = \begin{bmatrix} \mathbf{I} \\ \mathbf{I} \end{bmatrix} \bar{\mathbf{y}}_c \quad (5)$$

Likewise we can write the relation between the excitation quantities at the coupling point of the two subsystems in relation to the uncoupled subsystem models and the synthesised model as

$$\bar{\mathbf{u}}_c = \begin{bmatrix} \mathbf{I} & \mathbf{I} \end{bmatrix} \begin{Bmatrix} \mathbf{u}_c^I \\ \mathbf{u}_c^{II} \end{Bmatrix} \quad (6)$$

and from here on considering coupling responses only in displacement,  $\mathbf{y}_c^i$  for simplicity. We can now write the state-space realisation on coupled form using Equations (4), (5) and 6, which is defined as

$$\begin{Bmatrix} \ddot{\bar{\mathbf{y}}}_c \\ \dot{\bar{\mathbf{y}}}_c \\ \dot{\mathbf{x}}_o \end{Bmatrix} = \begin{bmatrix} \mathbf{A}_{vv}^i & \mathbf{A}_{vd}^i & \mathbf{A}_{vo}^i \\ \mathbf{I} & 0 & 0 \\ 0 & \mathbf{A}_{od}^i & \mathbf{A}_{oo}^i \end{bmatrix} \begin{Bmatrix} \dot{\bar{\mathbf{y}}}_c \\ \bar{\mathbf{y}}_c \\ \mathbf{x}_o \end{Bmatrix} + \begin{bmatrix} \mathbf{B}_{vv}^i & \mathbf{B}_{vo}^i \\ 0 & 0 \\ 0 & \mathbf{B}_{oo}^i \end{bmatrix} \begin{Bmatrix} \bar{\mathbf{u}}_c \\ \mathbf{u}_o \end{Bmatrix} \quad (7a)$$

$$\begin{Bmatrix} \bar{\mathbf{y}}_c \\ \mathbf{y}_o \end{Bmatrix} = \begin{bmatrix} 0 & \mathbf{I} & 0 \\ \mathbf{C}_{ov}^i & \mathbf{C}_{od}^i & \mathbf{C}_{oo}^i \end{bmatrix} \begin{Bmatrix} \dot{\bar{\mathbf{y}}}_c \\ \bar{\mathbf{y}}_c \\ \mathbf{x}_o \end{Bmatrix} \quad (7b)$$

The advantage of using first-order state-space models in lieu to a second-order modal model is that the state-space model has lesser restriction which enables this model to better reproduce the measured data. However, some physical properties, introduced as constraints in the system identification phase, have been found to enhance the first-order state-space model, [5]. To enforce these kinematic and equilibrium constraints we first need to transform the two sub-components, subsystem I and subsystem II, in to coupling form in accordance with equations (7a) and (7b). The first kinematic constraint to enforce is that the interface velocities and displacements should be equal. This is done by considering the first row of Equation (7a) from which we have that

$$\ddot{\bar{\mathbf{y}}}_c^I = \mathbf{A}_{vv}^I \dot{\bar{\mathbf{y}}}_c^I + \mathbf{A}_{vd}^I \bar{\mathbf{y}}_c^I + \mathbf{A}_{vo}^I \mathbf{x}_o^I + \mathbf{B}_{vv}^I \bar{\mathbf{u}}_c^I + \mathbf{B}_{vo}^I \mathbf{u}_o^I \quad (8a)$$

$$\ddot{\bar{\mathbf{y}}}_c^{II} = \mathbf{A}_{vv}^{II} \dot{\bar{\mathbf{y}}}_c^{II} + \mathbf{A}_{vd}^{II} \bar{\mathbf{y}}_c^{II} + \mathbf{A}_{vo}^{II} \mathbf{x}_o^{II} + \mathbf{B}_{vv}^{II} \bar{\mathbf{u}}_c^{II} + \mathbf{B}_{vo}^{II} \mathbf{u}_o^{II} \quad (8b)$$

and to fulfil the stated kinematic constraints it follows that

$$\dot{\bar{\mathbf{y}}}_c^I = \dot{\bar{\mathbf{y}}}_c^{II} \stackrel{def}{=} \dot{\bar{\mathbf{y}}}_c \quad (9a)$$

$$\bar{\mathbf{y}}_c^I = \bar{\mathbf{y}}_c^{II} \stackrel{def}{=} \bar{\mathbf{y}}_c \quad (9b)$$

and the equilibrium conditions are met by

$$\bar{\mathbf{u}}_c^I = \bar{\mathbf{u}}_c^{I,II} + \bar{\mathbf{u}}_{c,e}^I \quad (10a)$$

$$\bar{\mathbf{u}}_c^{II} = -\bar{\mathbf{u}}_c^{I,II} + \bar{\mathbf{u}}_{c,e}^{II} \quad (10b)$$

where  $\bar{\mathbf{u}}_c^{I,II}$  denotes the cross-sectional force between the two subsystems and  $\bar{\mathbf{u}}_{c,e}^{II}$  denotes the externally applied force to the interface DOFs. By introducing Equations (9a) and (10a) into (8a) and Equations (9b) and (10b) into (8b) we get

$$\ddot{\bar{\mathbf{y}}}_c = \mathbf{A}_{vv}^I \dot{\bar{\mathbf{y}}}_c + \mathbf{A}_{vd}^I \bar{\mathbf{y}}_c + \mathbf{A}_{vo}^I \mathbf{x}_o^I + \mathbf{B}_{vv}^I \bar{\mathbf{u}}_c^{I,II} + \mathbf{B}_{vv}^I \bar{\mathbf{u}}_{c,e}^I + \mathbf{B}_{vo}^I \mathbf{u}_o^I \quad (11a)$$

$$\ddot{\bar{\mathbf{y}}}_c = \mathbf{A}_{vv}^{II} \dot{\bar{\mathbf{y}}}_c + \mathbf{A}_{vd}^{II} \bar{\mathbf{y}}_c + \mathbf{A}_{vo}^{II} \mathbf{x}_o^{II} + \mathbf{B}_{vv}^{II} \bar{\mathbf{u}}_c^{I,II} + \mathbf{B}_{vv}^{II} \bar{\mathbf{u}}_{c,e}^{II} + \mathbf{B}_{vo}^{II} \mathbf{u}_o^{II} \quad (11b)$$

The mass inertia of the interface DOFs correspond to the inverse of  $\mathbf{B}_{vv}^I$  and  $\mathbf{B}_{vv}^{II}$ . To introduce these kinematic constraints the first step is to multiply Equation (11a) with  $(\mathbf{B}_{vv}^I)^{-1}$  from the left and Equation (11b) with  $(\mathbf{B}_{vv}^{II})^{-1}$  also from the left and add them together as

$$\begin{aligned} \left( (\mathbf{B}_{vv}^I)^{-1} + (\mathbf{B}_{vv}^{II})^{-1} \right) \ddot{\bar{\mathbf{y}}}_c &= \left( (\mathbf{B}_{vv}^I)^{-1} \mathbf{A}_{vv}^I + (\mathbf{B}_{vv}^{II})^{-1} \mathbf{A}_{vv}^{II} \right) \dot{\bar{\mathbf{y}}}_c \\ &+ \left( (\mathbf{B}_{vv}^I)^{-1} \mathbf{A}_{vd}^I + (\mathbf{B}_{vv}^{II})^{-1} \mathbf{A}_{vd}^{II} \right) \bar{\mathbf{y}}_c \\ &+ (\mathbf{B}_{vv}^I)^{-1} \mathbf{A}_{vo}^I \mathbf{x}_o^I + (\mathbf{B}_{vv}^{II})^{-1} \mathbf{A}_{vo}^{II} \mathbf{x}_o^{II} \\ &+ \bar{\mathbf{u}}_c + (\mathbf{B}_{vv}^I)^{-1} \mathbf{B}_{vo}^I \mathbf{u}_o^I \\ &+ (\mathbf{B}_{vv}^{II})^{-1} \mathbf{B}_{vo}^{II} \mathbf{u}_o^{II} \end{aligned} \quad (12)$$

Here  $\bar{\mathbf{u}}_c$  is the total external load applied to assembled components interface DOFs and is defined as

$$\bar{\mathbf{u}}_c \stackrel{def}{=} \bar{\mathbf{u}}_c^I + \bar{\mathbf{u}}_c^{II} = \bar{\mathbf{u}}_c^{I,II} + \bar{\mathbf{u}}_{c,e}^I - \bar{\mathbf{u}}_c^{I,II} + \bar{\mathbf{u}}_{c,e}^{II} = \bar{\mathbf{u}}_{c,e}^I + \bar{\mathbf{u}}_{c,e}^{II} \quad (13)$$

Rearranging Equation (12) slightly we can write it as

$$\ddot{\bar{\mathbf{y}}}_c = \mathbf{A}_{vv} \dot{\bar{\mathbf{y}}}_c + \mathbf{A}_{vd} \bar{\mathbf{y}}_c + \mathbf{A}_{vo}^I \mathbf{x}_o^I + \mathbf{A}_{vo}^{II} \mathbf{x}_o^{II} + \mathbf{B}_{vv} \bar{\mathbf{u}}_c + \mathbf{B}_{vo}^I \mathbf{u}_o^I + \mathbf{B}_{vo}^{II} \mathbf{u}_o^{II} \quad (14)$$

With

$$\bar{\mathbf{A}}_{vv} = \mathbf{B}_{vv}^{II} \left( \mathbf{B}_{vv}^I + \mathbf{B}_{vv}^{II} \right)^{-1} \mathbf{A}_{vv}^I + \mathbf{B}_{vv}^I \left( \mathbf{B}_{vv}^I + \mathbf{B}_{vv}^{II} \right)^{-1} \mathbf{A}_{vv}^{II} \quad (15)$$

$$\bar{\mathbf{A}}_{vd} = \mathbf{B}_{vv}^{II} \left( \mathbf{B}_{vv}^I + \mathbf{B}_{vv}^{II} \right)^{-1} \mathbf{A}_{vd}^I + \mathbf{B}_{vv}^I \left( \mathbf{B}_{vv}^I + \mathbf{B}_{vv}^{II} \right)^{-1} \mathbf{A}_{vd}^{II} \quad (16)$$

$$\bar{\mathbf{A}}_{vo}^I = \mathbf{B}_{vv}^{II} \left( \mathbf{B}_{vv}^I + \mathbf{B}_{vv}^{II} \right)^{-1} \mathbf{A}_{vo}^I \quad (17)$$

$$\bar{\mathbf{A}}_{vo}^{II} = \mathbf{B}_{vv}^{II} \left( \mathbf{B}_{vv}^I + \mathbf{B}_{vv}^{II} \right)^{-1} \mathbf{A}_{vo}^{II} \quad (18)$$

$$\bar{\mathbf{B}}_{vv} = \mathbf{B}_{vv}^I \left( \mathbf{B}_{vv}^I + \mathbf{B}_{vv}^{II} \right)^{-1} \mathbf{B}_{vv}^{II} \quad (19)$$

$$\bar{\mathbf{B}}_{vo}^I = \mathbf{B}_{vv}^I \left( \mathbf{B}_{vv}^I + \mathbf{B}_{vv}^{II} \right)^{-1} \mathbf{B}_{vo}^{II} \quad (20)$$

$$\bar{\mathbf{B}}_{vo}^{II} = \mathbf{B}_{vv}^I \left( \mathbf{B}_{vv}^I + \mathbf{B}_{vv}^{II} \right)^{-1} \mathbf{B}_{vo}^{II} \quad (21)$$

the assembled systems on state-space form can now be written on matrix form as

$$\begin{aligned} \begin{Bmatrix} \ddot{\bar{\mathbf{y}}}_c \\ \dot{\bar{\mathbf{y}}}_c \\ \dot{\mathbf{x}}_o^I \\ \dot{\mathbf{x}}_o^{II} \end{Bmatrix} &= \begin{bmatrix} \bar{\mathbf{A}}_{vv} & \bar{\mathbf{A}}_{vd} & \bar{\mathbf{A}}_{vo}^I & \bar{\mathbf{A}}_{vo}^{II} \\ \mathbf{I} & \mathbf{0} & \mathbf{0} & \mathbf{0} \\ 0 & \bar{\mathbf{A}}_{od}^I & \bar{\mathbf{A}}_{oo}^I & \mathbf{0} \\ 0 & \bar{\mathbf{A}}_{od}^{II} & \mathbf{0} & \bar{\mathbf{A}}_{oo}^{II} \end{bmatrix} \begin{Bmatrix} \dot{\bar{\mathbf{y}}}_c \\ \bar{\mathbf{y}}_c \\ \mathbf{x}_o^I \\ \mathbf{x}_o^{II} \end{Bmatrix} \\ &+ \begin{bmatrix} \bar{\mathbf{B}}_{vv} & \bar{\mathbf{B}}_{vo}^I & \bar{\mathbf{B}}_{vo}^{II} \\ 0 & \mathbf{0} & \mathbf{0} \\ 0 & \bar{\mathbf{B}}_{oo}^I & \mathbf{0} \\ 0 & \mathbf{0} & \bar{\mathbf{B}}_{oo}^{II} \end{bmatrix} \begin{Bmatrix} \bar{\mathbf{u}}_c \\ \mathbf{u}_o^I \\ \mathbf{u}_o^{II} \end{Bmatrix} \end{aligned} \quad (22a)$$

$$\begin{Bmatrix} \bar{\mathbf{y}}_c \\ \mathbf{y}_o^I \\ \mathbf{y}_o^{II} \\ \mathbf{y}_o \end{Bmatrix} = \begin{bmatrix} 0 & \mathbf{I} & \mathbf{0} & \mathbf{0} \\ \mathbf{C}_{ov}^I & \mathbf{C}_{od}^I & \mathbf{C}_{oo}^I & \mathbf{0} \\ \mathbf{C}_{ov}^{II} & \mathbf{C}_{od}^{II} & \mathbf{0} & \mathbf{C}_{oo}^{II} \end{bmatrix} \begin{Bmatrix} \dot{\bar{\mathbf{y}}}_c \\ \bar{\mathbf{y}}_c \\ \mathbf{x}_o^I \\ \mathbf{x}_o^{II} \end{Bmatrix} \quad (22b)$$

For the system studied in this paper which is a non-gyroscopic, non-circulatory and passive mechanical system it is expected that Betti's reciprocity principle should apply. To ensure reciprocity the condition  $\mathbf{C}^i \mathbf{B}^i = 0$  has been enforced, in order for the system to be self-adjoint. The state-space models used have also been forced to be stable and passive, see [5].

### 3 System set-up

The purpose of the investigation is to investigate the causal effects different factors have on the tool tip FRF which is the foundation for the stability lobe chart. This approach requires a system which is free from deficiencies, such as noise and model order uncertainties. The system chosen for this investigation is a simplified FE-model of a test rig used in [4], see Figure 2.

The FE-model of the test rig consists of two substructures, see Figure 3. The spring suspended metal block with the clamping unit along with the coupling and the tool family generic part of the cutting tool, referred to as the blank, constitutes subsystem I. The tool tip, with a geometry that may vary within the tool family, is considered to be substructure II. Figure 4 shows the DOF numbering of the interface. In this study we are particularly interested in motion in the y- and z-directions, DOFs 2 and 3.

Before proceeding with sensitivity analysis we made a validation of the coupling technique. As a reference we obtained frequency response functions of the total system coupled to an entity by ordinary FEM assembly procedures. We see one example in Figure 5. To mimic the system identification procedures for test data we made a system identification of FRFs given by FEM analysis of substructure I. In the frequency range from 0 to 5 kHz it was found that 30 states were sufficient to capture data. In the FE representation 0.5 percent relative viscous damping was introduced to all modes.

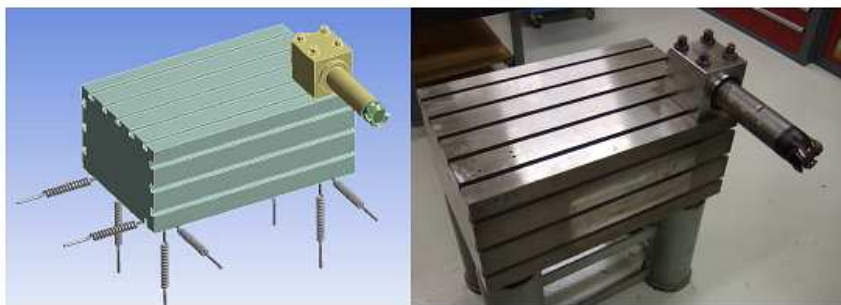


Figure 2: Left; FE-model of test rig. Right; real test rig.

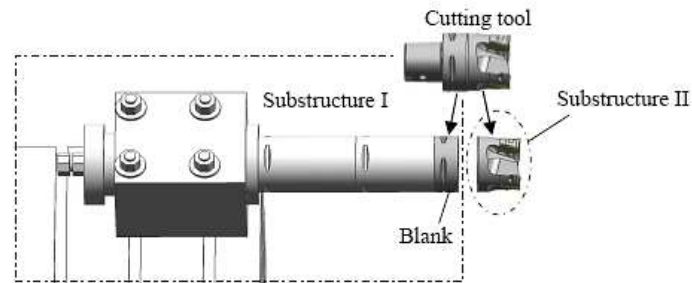


Figure 3: Substructures I and II.

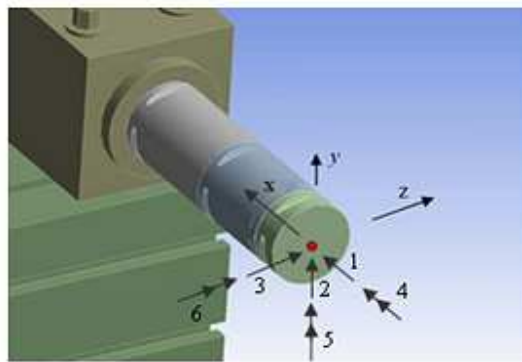


Figure 4: Reference coordinate system and degree of freedom notations.

## 4 Sensitivity analysis and evaluation method

With a reliable identification process in place the next step is the sensitivity analysis based on perturbation of the state space model from modal data and model estimation of that system.

### 4.1 Problem formulation

The evaluation is limited to investigate the factors governing the accuracy of the predicted spindle speed and depth of cut and *quantify* the impact they have on the predicted stability lobes. A criterion function based on the stability lobe chart is required. The sensitivity analysis is performed through a screening process where each parameter can vary within a certain interval. Each test combination resulted in a perturbed FRF from which a stability lobe chart were obtained. The lobes from the perturbed test were evaluated against a stability lobe chart based on the solution of the unperturbed coupled state space model presented in Figure 5 system based on two criteria.

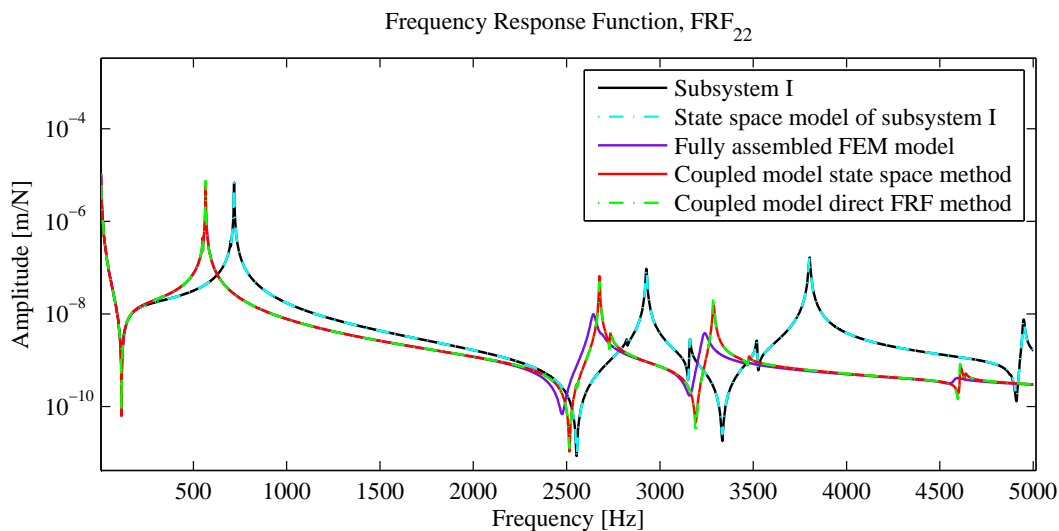


Figure 5: Frequency response function comparison between uncoupled subsystem I and the state space identification of subsystem I as well as the fully assembled FEM model and the assembled substructures using state space and direct FRF coupling technique of the y-direction direct FRF, the  $FRF_{22}$ .

A first criterion is an evaluation of the angle between stability lobe data vectors of the nominal and perturbed systems. These data vectors are stability lobe function samples at discrete spindle speeds. The good thing about this approach is that amplitude of the vectors is disregarded. The angle ranges between 0 and  $\pi/2$  where 0 means that the two data vectors are completely parallel and an angle of  $\pi/2$  means that the two data vectors are orthogonal. In this evaluation the angle is normalised by taking cosine of the angle resulting in a number ranging from 0 to 1 where 1 means that the two data vectors are perfectly parallel and in that sense equal and 0 means completely orthogonal which is not desirable. We call this normalised angle the co-linearity index.

A second evaluation criterion is the minimum axial depth of cut,  $a_p^{lim}$ , where the cutting process is stable for all spindle speeds, see Figure 6. This criterion was selected since this depth of cut is the local minimum value of all lobes. This is not the case with the stability peaks which grows with higher spindle speeds. The minimum depth of cut is also the parameter that is especially important when machining at low spindle speeds.

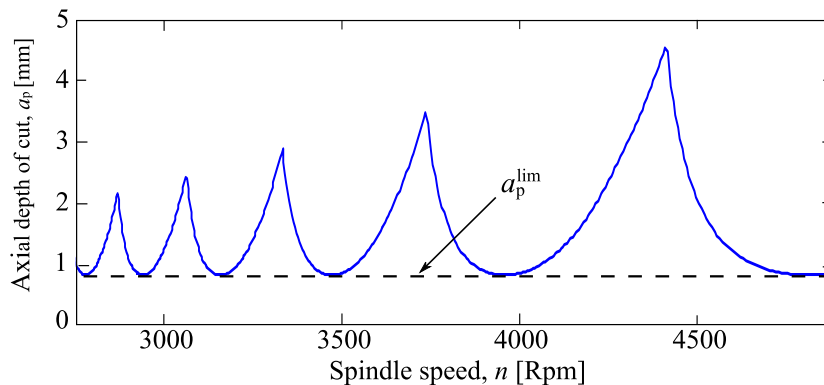


Figure 6: Description of minimum axial depth of cut,  $a_p^{lim}$ .

## 4.2 Screening

A traditional screening set up, see [16], is an essential first step of the objective evaluation method that will be used to answer the question of which factors has the largest impact on the criterion function and if there are any interaction between these factors. The aim is to assign all factors the same possibility to influence the criteria and then, if possible, reduce the number factors for further investigations. Some of the factors subjected to investigation in this paper have been found to have a strong non-linear behaviour within their range of variation. To add additional states or exclude states for instance will not result in a linearly dependent error between the results. This makes them unsuitable for the coupled analysis, proposed in [16], which would make it hard to determine their separate impact on the coupled system. A simple approach was taken regarding the sensitivity analysis. The approach was to change one parameter at the time and keep all others at their reference values. The screening procedure starts with listing factors, categorizing them and determine a relevant range of variation of each factor. Table 1 presents the factors chosen in this investigation along with their category and variation span. The screening procedure has multiple objectives. The first is to get an insight of which factors have most influence on the result of the coupled model. If a factor is found to have no influence on the criteria then that result is also useful information. The exclusion of a factor can be proven to be very beneficial from a time or economical perspective. The screening also ranks each factor and therefore gives an indication of which of the factors to put additional focus on.

The chosen factors all contribute differently to the identified models. The number of states included in the state-space model is an interesting parameter to investigate. Previous tests conducted in [17] showed that too few states

Table 1: Factors subjected to perturbation in identification of subsystem I. The nominal values of the reference system were 4 complex conjugated states, 0.5% damping and a upper limit frequency of 5000 Hz

<b>Trial nr</b>	<b>Factor</b>	<b>Change</b>
N1	Nr. of states to estimate first bending mode	Add 2 states
N2	Nr. of states to estimate first bending mode	Subtract 2 states
N3	Damping estimation of first bending mode	0.6%
N4	Damping estimation of first bending mode	0.4%
N5	FRF magnitude	Add 10%
N6	FRF magnitude	Subtract 10%
N7	Upper limit frequency	2000 Hz

could influence the coupled systems of but no investigation of the impact of too many states was made. Damping is another parameter of interest since it can normally not be precisely determined from measurements. To see how much frequency response function amplitude error influences the coupled system is also of interest. This parameter can be influenced from ill-calibrated accelerometers, errors in force input measurements and test set-up errors. The upper limit frequency of the FRFs will determine how many modes that are taken into account by the state-space substructures and this has effect on the coupled system.

### 4.3 Results

The stability lobe chart is constructed from the real part of  $FRF_{22}$  and  $FRF_{33}$ , which are the FRFs associated to transversal motion. Both these directions are important for the final evaluation of the stability lobe chart. The results of a comparison between the real part of the  $FRF_{22}$  of the reference and the perturbed systems show how the different parameter influences the location of the bending eigenfrequency and the amplitude of the  $FRF_{22}$ , see Figure 7.

Stability lobes for comparison were constructed based on the results of the perturbed FRFs for evaluation. The cutting parameters used to obtain the stability lobe charts are presented in Table 2.

Figure 8 shows how the different parameter settings affect the stability lobe

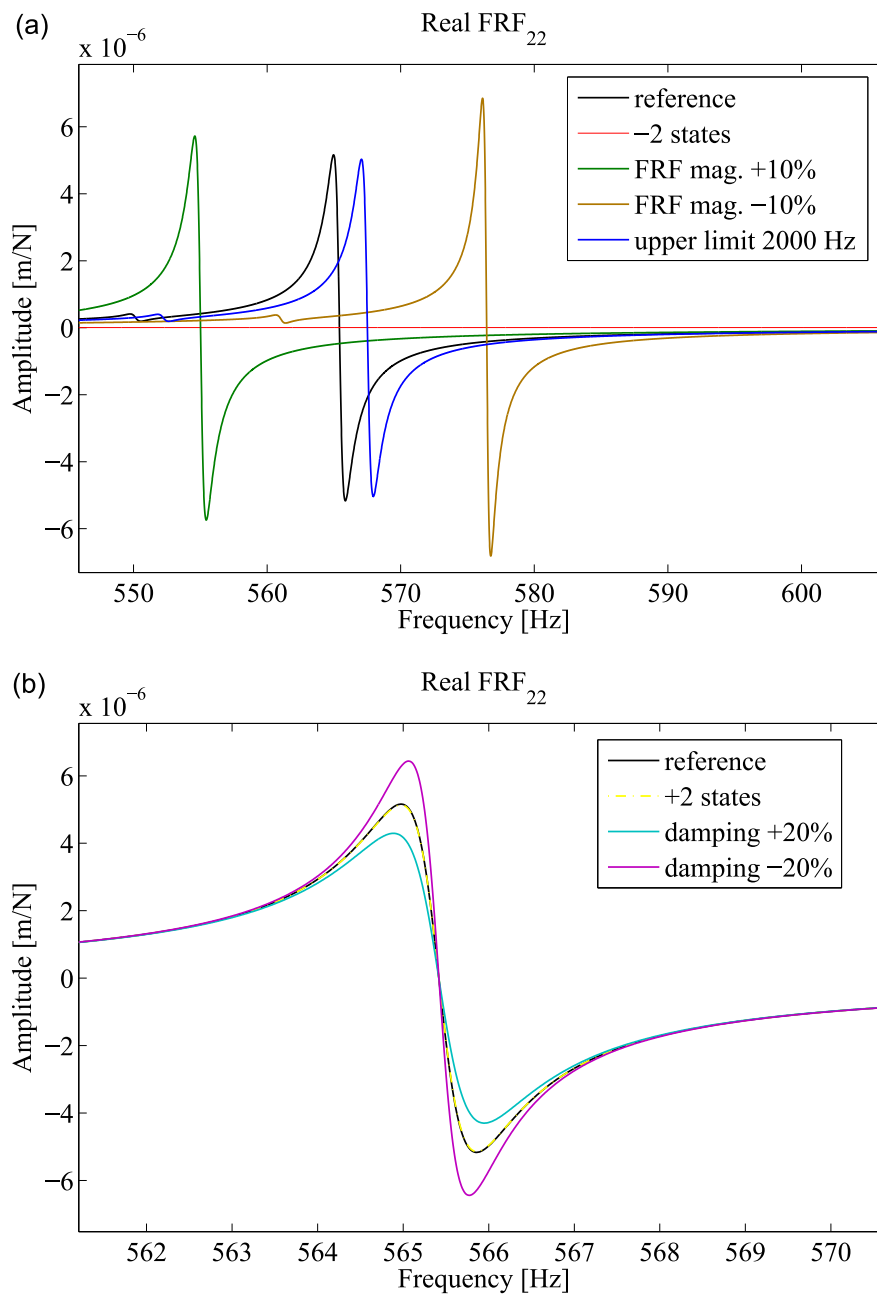


Figure 7: Real part of  $FRF_{22}$  of unperturbed (reference) and the perturbed systems. Figure 7a consists of a comparison between the reference system and the four most influential perturbed systems and Figure 7b shows a zoomed view of the first bending mode and the results from the three least influential parameter changes.

Table 2: Cutting parameters used in simulation of stability lobes

Cutting parameters	Quantity	Unit
Number of teeth, $z$	1	—
Tool diameter, $D_c$	80	[mm]
Radial width of cut, $a_e$	80	[mm]
Cutting force coefficient in tangential direction, $K_t$	1319	[MPa]
Cutting force coefficient in radial direction, $K_r$	789	[MPa]

chart. It should be noted that the perturbed system with a reduced number of states is not seen in the chosen plot interval. The amplitude of the stability lobes for this setting is much too high to be included in the plot. The drastic impact of this setting is seen in Figure 7.

The plotted stability lobe chart comparison gives a good indication of the influence of different perturbations to the system but it makes it hard to quantify its meaning. The results of the comparisons of the angle between stability lobe data vectors and the minimum value of the depth of cut for each perturbed system compared to the reference system makes it easier to interpret the results. Such results are presented in Table 3.

From the results in Table 3 it can be seen that the factor with the smallest impact on the system is the one where two additional states has been introduced to add a resonance frequency close to that of the first bending mode. This factor has a very small influence on the angle between the real FRF vectors and almost no influence on the minimum amplitude value compared to the reference. The perturbed system where the state order had been underestimated by neglecting a bending mode showed a drastic impact on both evaluation criteria. The damping perturbation proved to give a very small influence on the subspace angle criterion and axial depth of cut seems to be proportional to the magnitude of the damping. A factor that influenced the coupled system much was the FRF magnitude. The magnitude increase by 10 percent gave an underestimation of the bending eigenfrequency by 12 Hz and an overestimation the eigenfrequency by 12 Hz with a magnitude decrease. Both these errors then propagated to the stability lobe chart resulting in an optimum spindle speed error of 90 rpm. The lowered upper limit frequency perturbation was the fourth least influential perturbation when it comes to the subspace angle index. The decreased upper limit frequency also gave a small axial depth-of-cut error.

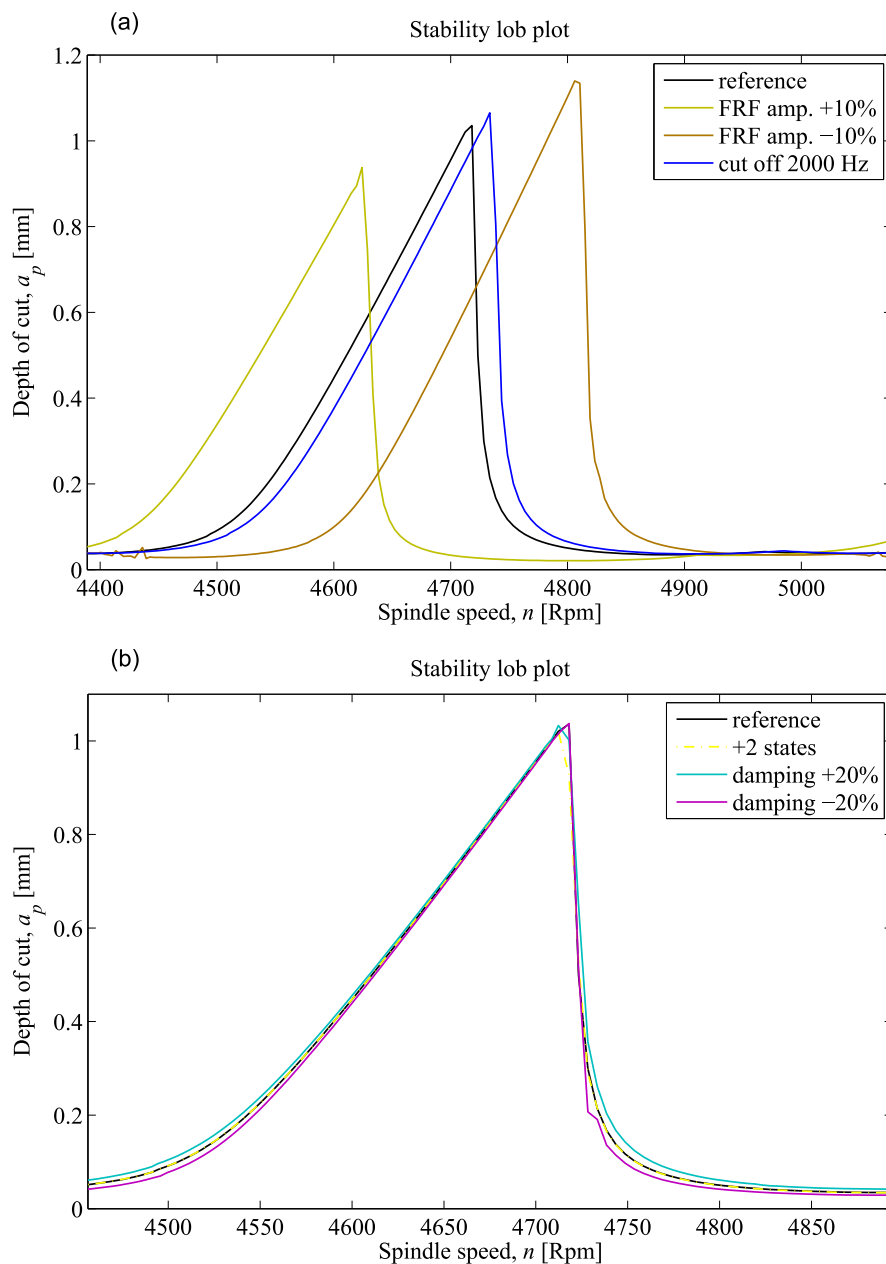


Figure 8: Stability lobe comparisons between unperturbed (reference) and the perturbed systems. Figure 8a consists of a comparison between the reference system and the three most influential perturbed systems, -2 states has been excluded from this figure because of the large amplitude deviation from the reference. Figure 8b shows a zoomed view of one stability lobe and the three least influential parameter changes compared to the reference.

Table 3: Comparison between the influences of the different perturbation factors co-linearity index and minimum axial depth of cut relative to that of reference configuration

Test nr	Co-linearity index	Relative axial depth of cut
N1	0.985	0.99
N2	0.410	1335.33
N3	0.975	1.21
N4	0.976	0.83
N5	0.484	0.60
N6	0.427	0.81
N7	0.825	1.06

## 5 Conclusions

The methodology and work flow used to conduct these analyses make up a good foundation for designing the measurement set-up. The approach with the evaluation criteria based on subspace angle between stability lobe data and minimum axial depth of cut, give the evaluation of the perturbed systems much clearer and the two evaluation criteria makes good indications on the comparison to the reference system. This method allows several factors to be evaluated against each other even though they can play a very different role in the identification process. Regarding the results, the sensitivity analysis definitely distinguishes the important from the less important parameters. The parameter that influenced the coupled system the most was an error in the estimation of the FRF amplitude and too few states. This indicates that great care must be taken both during the measurement procedure and the system identification. Accelerometer calibration errors of 5 percent is not uncommon for accelerometers used in these types of measurements. Large accelerometer errors can be expected from temperature transients, calibration errors, linearity errors, frequency and phase response errors, ageing errors, cable motion, and electromagnetic interference in cables. Load cell errors affects the FRF estimation similarly. It is seen that the number of states may be very important. This is much in line with the conclusions drawn in [17]. It seems that an excessive state order not necessarily causes bad coupling results. The damping perturba-

tion seems to influence only the axial depth of cut error in the stability chart. This is good from an application standpoint were the accurate spindle speed optimisation is considered much more important than an accurate prediction of the axial depth of cut presented in the stability chart. To find the stability limit is fairly easy to do at the production site compared to finding the optimum spindle speed. Regarding the upper limit frequency it is shown that it influences the coupled model but it does not have a large impact as long as no important states are disregarded as a consequence.

## References

- [1] Y. Altintas. *Manufacturing Automation: Metal Cutting Mechanics, Machine Tool Vibrations and CNC Design*. Cambridge University Press, 2000.
- [2] J. Tlustý and M. Poláček. The stability of machine tools against self excited vibrations in machining. *International Research in Production Engineering*, ASME:465–474, 1963.
- [3] S. A. Tobias. *Machine Tool Vibrations*. Blackie and Sons Ltd., 1965.
- [4] A. Liljehrn, A. Johansson and T. Abrahamsson. Dynamic substructuring in metal cutting machine chatter. In *Proceedings of ISMA2010 International Conference on Noise and Vibration Engineering Including USD2010*, pages 1915–1927. Leuven (Belgium), 2010.
- [5] P. Sjövall and T. Abrahamsson. Component system identification and state-space model synthesis. *Mechanical Systems and Signal Processing*, 21(7):2697–2714, 2007.
- [6] B. Jetmundsen, R. L. Bielawa and W.G. Flannelly. Generalized frequency domain substructure synthesis. *Journal of the American Helicopter Society*, 33(1):55–64, 1988.
- [7] S. S. Park, Y. Altintas, and M. Movahhedy. Receptance coupling for end mills. *International Journal of Machine Tools and Manufacture*, 43(9):889–896, 2003.
- [8] R. L. Bielawa J. H. Gordis and W. G. Flannelly. A General Theory for Frequency Domain Structural Synthesis, *Journal of Sound and Vibration*. *Journal of Sound and Vibration*, 150(1):139–158, 1998.
- [9] W. Liu and D. J. Ewins. Substructure synthesis via elastic media. *Journal of Sound and Vibration*, 257(2):361–379, 2002.

- [10] T. Lim. A Theoretical and Computational Study of the FRF-Based Substructuring Technique Applying Enhanced Least Square and Tsvd Approaches. *Journal of Sound and Vibration*, 231(4):1135–1157, 2000.
- [11] Y. Ren and C.F. Beards. On substructure synthesis with frf data. *Journal of Sound and Vibration*, 185(5):845–866, 1995.
- [12] R.R. Craig, Jr. and M. C. C. Bampton. Coupling of substructures for dynamic analysis. *AIAA Journal*, 6(7):1313–1319, 1968.
- [13] D. J. Rixen. A dual Craig-Bampton method for dynamic substructuring. *Journal of Computational and Applied Mathematics*, 168(1-2):383–391, 2004.
- [14] C. W. Jen, D. A. Johnson, and F. Dubois. Numerical modal analysis of structures based on a revised substructure synthesis approach. *Journal of Sound and Vibration*, 180(2):185–203, 1995.
- [15] E. Balmes. Use of generalized interface degrees of freedom in component mode synthesis. In *International Modal Analysis Conference IMAC. SEM*, Bethel, CT, USA, 1996.
- [16] L. Eriksson, E. Johansson, N. Kettaneh-Wold, C. Wikström, and S. Wold. Design of experiments: principles and applications. *Umetrics AB Learnways AB Stockholm Sweden*, page 425, 2008.
- [17] P. Sjövall, T. McKelvey and T. Abrahamsson. Constrained State-Space System Identification with Application to Structural Dynamics. *Automatica*, 42:1539–1546, 2006.